

Polymer Processing and Rheology

Polymer melts and concentrated solutions exhibit both viscous and elastic properties. The viscoelastic properties of polymeric solids were the principal topics of discussion in Chapter 5. In this chapter, the viscoelastic properties of polymer melts and concentrated solutions, particularly in relation to polymer-processing operations, are described. Viscous properties determine such processing parameters as the form of the velocity profile, the magnitude of the pressure drop, and the amount of heat generation (i.e., viscous heating) during extrusion through a die. Elastic behavior is responsible for such extrusion phenomena as die swell, melt fracture, and nonzero exit pressure. The fundamentals of polymer-processing operations and the basics of polymer rheology are presented in this chapter.

11.1 Basic Processing Operations

Polymer-processing operations may be classified into five broad categories—extrusion, molding, spinning, calendering, and coating. Of these, extrusion is perhaps the most widely used. Applications of extrusion include the continuous production of plastic pipe, sheet, and rods. Molding is normally a batch process, principally in the form of injection- and compression-molding operations used to make plastic parts as diverse as the cap to a ballpoint pen and a fiber-reinforced bathtub. Other important processing methods include the fiber spinning of textiles (discussed in Section 8.2.4), the calendering of plastic sheet, and the deposition of organic coatings on plastic sheet. Two specialized methods of preparing fiber-reinforced composites—filament winding and pultrusion—were discussed in Chapter 7.

11.1.1 Extrusion

A form of extrusion was probably first used in England at the end of the eighteenth century to produce seamless lead pipe. In 1845, a ram-driven device was used to extrude threads of gutta percha and to produce pipe from shellac and gutta percha. The first submerged cable laid across the English Channel in 1851 was an insulated copper conductor produced by what may be the first application of a commercial wire-coating operation. Screw-driven extruders were developed in the second half of the nineteenth century, and twin-screw extruders appeared in the late 1930s.

The two principal components of an extrusion operation are the extruder and the die. As illustrated in Figure 11-1, the extruder consists of a hopper that holds the resin stock (usually in the form of small pellets or powder) and the extruder barrel, which can be conceptually divided into three sections on the basis of function. These are called the *feed*, *compression*, and *metering* sections. In the feed section, the solid feed is conveyed by the rotating screw from the hopper to the compression zone where the resin begins to melt due to the action of electrical heaters attached to the barrel wall. By the time the resin reaches the metering zone all the resin has melted, and the shearing action of the screw rotating against the inner wall of the extruder barrel forces the melt out of the extruder and through a die. The die shapes the extrudate to the desired form. For example, a die with an opening in the form of an annulus (i.e., two concentric cylinders) is used to extrude pipe; a capillary die is used to extrude rods; and a slit die having a rectangular opening is used to extrude sheet. A specially designed capillary die is used to coat wire with a layer of plastic insulation (see Section 11.5.2).

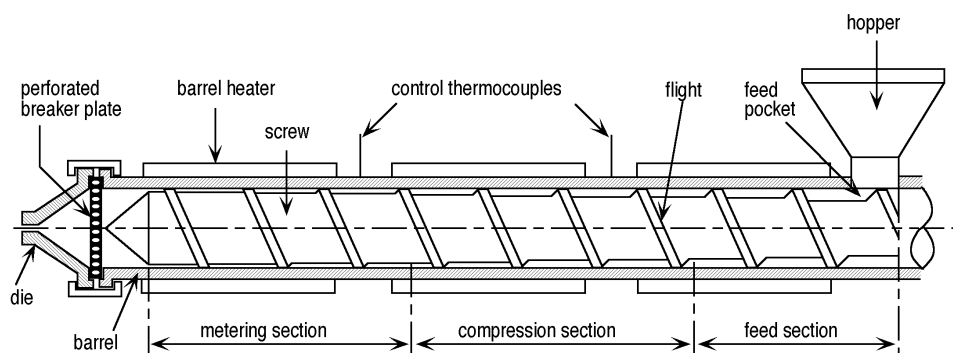


Figure 11-1 Illustration of a single-screw extruder. Adapted from N. G. McCrum, C. P. Buckley, and C. B. Bucknall, *Principles of Polymer Engineering*, 1988, Oxford: Oxford University Press.

In commercial polymer production, powder from a polymerization reactor may be fed directly to an extruder that has an opening for venting volatiles—a process called *devolatilization*. Examples of volatile contaminants include residual monomer and solvent that may be used during the polymerization process. The extruded melt is then passed through a capillary die, cooled, and chopped to form small pellets. These pellets are easier and safer to handle than the powder and can be shipped, stored, dried, and finally fed into the hopper of another extruder or injection-molding machine to produce the final product.

The extruder illustrated in Figure 11-1 has a single screw that is tapered so that the distance between the bottom of the screw channel and the wall of the barrel decreases as the metering section is reached. This provides increasing shear rate (see Section 11.5.1) as the melt is forced toward the exit of the extruder. This is advantageous since the viscosity of polymer melts and concentrated polymer solutions decreases with increasing shear rate, as discussed in Section 11.2.1. Extruders equipped with twin screws that rotate in opposite directions are used when even higher shear rates are needed, as in the case of temperature-sensitive, high-viscosity polymer melts.

11.1.2 Molding

Molding is one of the earliest and most important processing operations. These include compression, transfer, injection, reaction injection, thermoforming, blow, and rotational molding, which are included in this section.

Compression Molding. In many ways, compression molding is the least expensive and simplest of all polymer-processing operations. An early form of compression molding was used by the ancient Chinese to form articles from papier-mâché. During the early nineteenth century, compression molding was used in the United States and other countries to mold rubber parts and cases made from a composite of gum shellac and woody fibers. In 1907, Leo Baekeland employed a compression-molding process to produce phenol-formaldehyde (i.e., phenolic) resins [1].

Today, compression molding and a related technique, transfer molding, are the principal methods of molding thermosets such as phenolic resins, alkyds, and unsaturated polyesters (see Section 9.3.2). Injection molding, described in the next section, is the preferred method for molding thermoplastics, except in the case of molding large parts where the cost of transfer molding or injection molding may be excessive compared to that of compression molding. The compression-molding process is fairly simple. First, the resin is placed in the bottom half of an open, heated mold. Next, the top half of the mold is placed over the bottom half and pressure is applied to cause the molten resin to completely fill the mold cavity, while the excess resin is forced out of the mold as *flash*. Presses with clamping capacities from 5 to 4000 tons are available for manual and semiautomatic operation. An illustration of a compression-molding operation is shown in Figure 11-2.

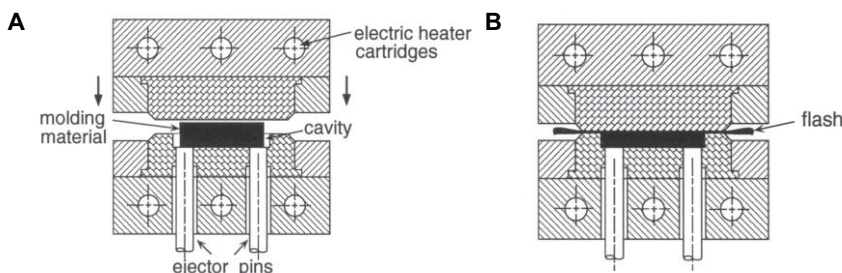


Figure 11-2 Compression-molding process. **A.** View of an open mold with molding material in place. **B.** Closed mold showing formed part and flash formed from excess resin. Adapted from J. L. Hull, Compression and Transfer Molding, in *The Concise Encyclopedia of Polymer Science and Engineering*, 1990. J. I. Kroschwitz, ed. Copyright © 1990 by John Wiley & Sons. This material is used by permission of John Wiley & Sons, Inc.

Transfer Molding. In the case of *transfer* (or *plunger*) molding, the mold is closed prior to resin entry. A simplified diagram of a transfer-molding process is shown in Figure 11-3. A plunger is used to force a predetermined amount of molten resin from an open *transfer pot* through a small opening in the mold. After the mold is opened (Figure 11-3C), ejector pins are used to push the molded part out of the mold. The residual (i.e., uninjectored molding resin) is called the *cull*. Molding cycles

tend to be shorter than for compression molding because mold temperatures can be higher and the premelted polymer flows more easily through the mold, typically under lower pressure. For these reasons, transfer molding is used to mold parts with intricate geometries and to mold fragile parts or when an insert is used in the mold and the flow of granular molding material during compression molding would otherwise damage or displace the insert.

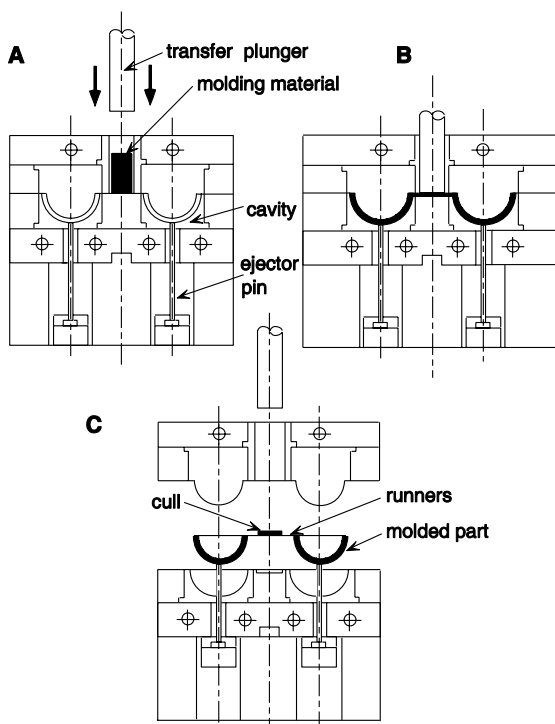


Figure 11-3 Transfer-molding operation. **A.** Transfer pot is loaded while mold is in closed position. **B.** Plunger pushes molding material into mold form. **C.** Mold opens and ejector pins push out molded part. Adapted from J. L. Hull, Compression and Transfer Molding, in *The Concise Encyclopedia of Polymer Science and Engineering*, 1990. J. I. Kroschwitz, ed. Copyright © 1990 by John Wiley & Sons. This material is used by permission of John Wiley & Sons, Inc.

In the case of molding thermoset resins, the molding compound is first placed in the cavity of the compression mold or the transfer pot of a transfer-molding process and heated (ca. 150°C) to provide sufficient flow for mold filling. Pressure (e.g., 2000 psi or 13.4 MPa) is then applied over sufficient time to allow the resin to cure (i.e., crosslink).

Injection Molding. Another important polymer-processing operation is injection molding. The principle behind injection molding dates back to 1856 when E. Pelouze of the United States developed a die-casting machine for forcing molten metal into a die by mechanical or hydraulic means. The development of the first injection-molding machine for thermoplastics was a result of ivory shortages during the Civil War. In 1868, the Phelan and Collender Co., a producer of billiard balls, offered an impressive award of \$10,000 to anyone who could produce a satisfactory substitute for ivory. In 1869, John Wesley Hyatt, a printer from Boston, invented the material celluloid (cellulose nitrate) to replace ivory. Celluloid was the world's first commercial synthetic resin and was used to produce products as diverse as billiard balls and dentures. In 1872, John and his brother Isaiah patented a simple extrusion device consisting of a steam-heated cylinder, a hydraulic plunger, and a discharge nozzle to extrude rods and tubes from cellulose nitrate.

As illustrated in Figure 11-4, one type of a modern injection-molding operation uses a reciprocating screw to melt a measured volume of feed introduced through the hopper. After a sufficient time has elapsed to form a homogeneous melt, the rotation of the screw ceases, and the melt is rammed into a mold under high pressure by a hydraulically driven thrust of the screw. The amount of resin that can be molded may vary with a particular machine from a few grams to a few kilograms, with clamping forces up to 5000 tons.

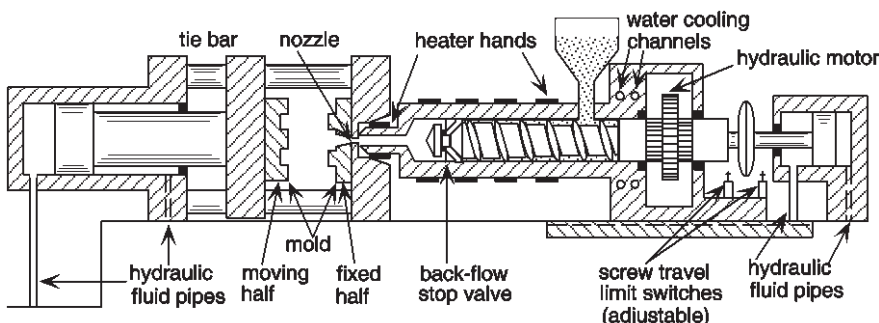


Figure 11-4 Illustration of a reciprocating-screw injection-molding machine and mold. Adapted from N. G. McCrum, C. P. Buckley, and C. B. Bucknall, *Principles of Polymer Engineering*. 1988, Oxford: Oxford University Press.

A mold may be used to produce a single part such as a computer keyboard or several smaller parts simultaneously (i.e., multi-impression molds). As an illustration, the cross section of a multi-impression mold to produce plastic boxes is shown in Figure 11-5A. The resulting molded assembly after removal from the mold is illustrated in Figure 11-5B. Anyone who has ever built a plastic model airplane is already familiar with the features of an injection-molded assembly. The thick sec-

tion through which the molten resin is forced from the nozzle of the injection-molding machine and first enters the mold is called the *sprue*. From the sprue, the melt is pushed through *runners*, which evenly distribute the melt to each mold cavity. The narrow point of attachment of the runner to the mold cavity is called the *gate*. After the mold is totally filled, it is cooled and opened to release the molded assembly. The molded parts are then broken from their attachment at the gates, and scrapped sprues, runners, and gates may be recycled to the molding operation. Molds must be able to withstand significant pressures and high temperatures and produce parts with close tolerances after numerous and rapid operations. For these reasons, great care must be exercised in mold design and manufacture. This usually represents a significant expenditure of capital, which contributes significantly to the total price of the molded part.

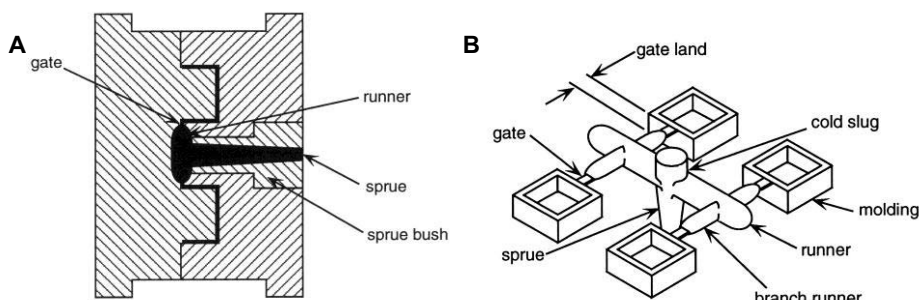


Figure 11-5 **A.** Typical mold design used in a multi-impression injection-molding process for the production of plastic boxes in this example. **B.** Removed mold assembly showing boxes and plastic scrap (i.e., sprue and runners). Adapted from N. G. McCrum, C. P. Buckley, and C. B. Bucknall, *Principles of Polymer Engineering*. 1988. Oxford: Oxford University Press.

There are several variations of the basic design of the reciprocating-screw injection-molding machine illustrated in Figure 11-4. For example, a less common design often used for thermoplastics is called the screw pot or *two-stage* screw. In this variation of the injection-molding process, the operations of the extruder screw and injection plunger are separated. A fixed (i.e., non-reciprocating) screw is used to melt the resin, which flows into a separate injection chamber and plunger assembly. The reciprocating-screw design is preferred for molding thermosets and elastomers and for heat-sensitive thermoplastics.

Reaction Injection Molding. Reaction injection molding or RIM is a relatively new process (developed in Germany during the late 1960s) whereby the polymer is simultaneously synthesized and molded into the finished product. An illustration of a RIM process is shown in Figure 11-6. At the start of the process, exact quanti-

ties of monomers (including catalyst and other additives) are metered into a mixing unit and rapidly forced into the mold, where most of the polymerization occurs. In contrast to injection molding, temperatures and clamping pressures in a RIM process are relatively low, allowing the use of inexpensive aluminum tooling. Other advantages of RIM include low energy consumption, rapid start-up time, and its suitability for the manufacture of large articles such as automotive bumpers. Disadvantages include the risk of worker exposure to noxious, high-vapor-pressure reagents such as diisocyanates, which are used in the RIM production of polyurethane.

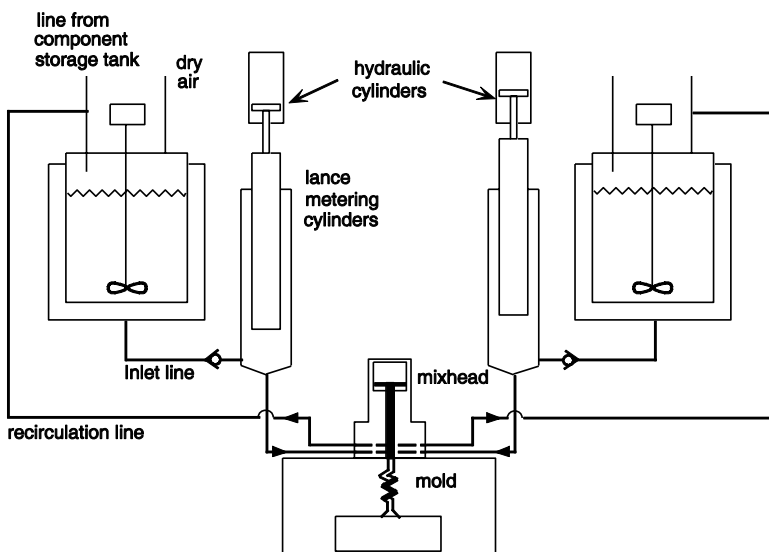


Figure 11-6 Illustration of a reaction injection-molding process showing separate tanks for polymerization reagents. Adapted from L. T. Manzione, Reaction Injection Engineering, in *The Concise Encyclopedia of Polymer Science and Engineering*, 1990. J. I. Kroschwitz, ed. Copyright © 1990 by John Wiley & Sons. This material is used by permission of John Wiley & Sons, Inc.

Due to the need for a controlled and rapid polymerization process, RIM is suited only for condensation-type polymers with favorable polymerization kinetics. Examples of polymers that can be processed in this way include polyamides, epoxies, and especially polyurethanes, which represent more than 95% of total RIM production. Polyurethanes are prepared by reacting diisocyanates with diols and chain extenders as discussed in Section 9.2.2. The majority of the RIM-produced polyurethane is used for elastomer applications (e.g., automotive bumpers and fascia), with the remainder used for structural foam. In addition, milled glass and short glass fi-

bers can be added during RIM to provide reinforcement to the molded part. This process, called reinforced RIM or RRIM, was developed in the 1970s.

Thermoforming. Thermoforming is an operation borrowed from metallurgy. In thermoforming, a plastic sheet is heated until it softens and is then formed to the shape of a mold preform by application of external air pressure or by pulling a vacuum (i.e., vacuum forming) between the sheet and the mold, as illustrated in Figure 11-7. Ancient Egyptian craftsmen who softened tortoise shells to form a variety of shapes may have been the first thermoformers, but it was not until 1938, with the production of blister packaging from cellulose acetate sheet, that the modern thermoforming industry began. Applications for thermoforming in today's plastics industry range from the high-volume production of plastic drinking cups to the production of plastic bed liners of half-ton pickup trucks.

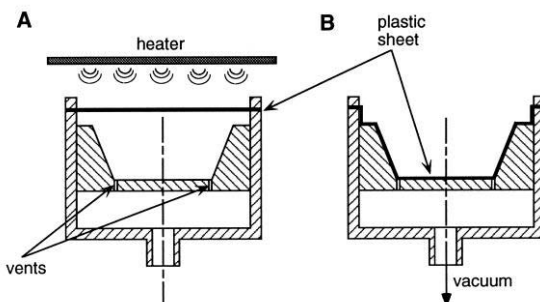


Figure 11-7 Vacuum-forming operation. **A.** Flat sheet is heated. **B.** Softened sheet is forced to fit the mold contour by evacuating the space between the sheet and the mold. Adapted from R. J. Crawford, *Plastics Engineering*. 1990, Danvers, MA: Elsevier Science, p. 200. Copyright 1981, with permission from Elsevier.

Blow Molding. Blow molding uses a gas (e.g., air or sometimes nitrogen) to expand a hot preform, or *parison*, against the form of a mold cavity to produce a hollow object. Blow molding may date back to 1880 when John Wesley Hyatt used this technique to produce baby rattles. Plastic bottles, automotive fuel tanks, toy tricycles, and other consumer products are made in this way. The first plastic bottle was blow-molded from polyethylene in 1943. Two types of processes are used for blow molding—*injection* and *extrusion*.

Injection blow molding is used primarily to produce small bottles and other parts. In this process, a parison is first injection-molded around a core rod in a preform mold and then transferred to a bottle blow-mold cavity. In the cavity, air expands the parison to the shape of the bottle.

For larger bottles and plastic tanks, an extrusion blow-molding process is used, as illustrated in Figure 11-8. In this process, the plastic resin is first extruded

as a tube (i.e., the parison) and is then captured by two halves of a mold in a continuous process. A blowpin is inserted, the mold is closed, and air is forced into the parison through the blowpin to expand the parison to the form of the mold cavity.

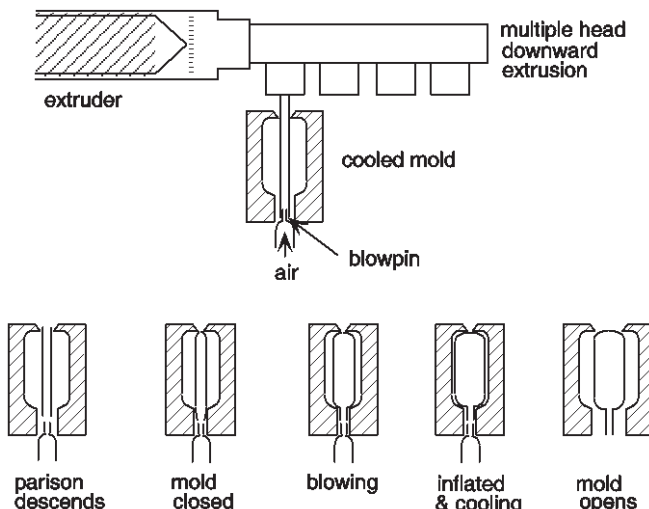


Figure 11-8 Extrusion blow-molding process in the production of plastic bottles. Adapted from D. H. Morton-Jones Kluwer, *Polymer Processing*. 1989, Kluwer Academic Publishers, Figures 6.1 and 6.2, p.128. Copyright 1989, D. H. Morton-Jones, Kluwer Academic Publishers.

Rotational Molding. Rotational molding, or rotomolding, uses centrifugal force to force-coat the inside of a mold with molten resin. The process is relatively simple, inexpensive to operate, and particularly suited for molding very large objects—the largest reported is an 85-m³ tank. The forerunner of the modern rotational-molding process was called slush molding, developed by the rubber industry to produce gloves, boots, and other items from plastisols. In slush molding, the liquid was first poured into a hot mold. Once the layer of plastic solidified, excess liquid was poured off.

In a typical rotational-molding operation, the mold cavity is first charged with a predetermined amount of resin powder or liquid. It is then closed and biaxially rotated in an oven. Finally, the mold is removed and cooled. Rotational molding produces little or no flash, thereby eliminating trimming operations and wasted resin. In addition, rotational molding produces very uniform wall thickness as well as strong corner sections, which may be difficult to obtain by other methods.

11.1.3 Calendering

Calendering is another method, in addition to extrusion, that can be used to produce plastic sheets. As illustrated in Figure 11-9, molten polymer is compressed in the small gap (the nip region) between two heated cylinders rotating in opposite directions. Sheets with widths up to 6 ft and a thickness as small as 0.002 in. can be produced at speeds up to 300 ft min⁻¹. The bulk of U.S. calendering output is poly(vinyl chloride) (PVC), including flexible sheet and film and blends and copolymers of PVC. Calenders can also be used to impart a finish (e.g., gloss or roughness) to a preformed plastic sheet or to laminate two sheets.

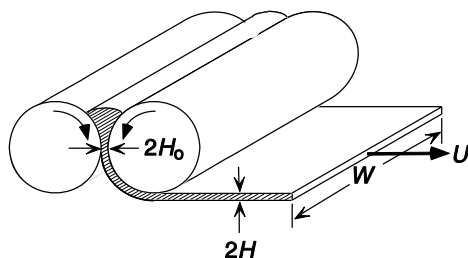


Figure 11-9 Simplified representation of a calendering process. Adapted from J. M. McKelvey, *Polymer Processing*. 1982, New York: John Wiley & Sons, with permission of the author.

11.1.4 Coating

Many different types of processes can be used to coat a thin layer of liquid (e.g., polymer melt or solution) onto a moving sheet, called the *web*. Examples of coatings include the deposition of

- Photographic emulsion on a cellulosic web
- Magnetic surface on poly(ethylene terephthalate) for recording and computer tape
- Polymer layer on a metal foil for capacitor applications
- Finishes and backings on textile fibers and fabrics

Examples of different coating operations are illustrated in Figure 11-10. In *roll coating* (Figure 11-10A), the lower roll picks up liquid from a bath and delivers it to a second roll or directly to the moving web. The thickness of the coating depends upon properties of the liquid (i.e., viscosity, etc.) and the spacing between the rolls

through which the web moves. This spacing may be controlled directly or indirectly by controlling pressure between the two rolls.

Another important type of coating operation is called *blade coating*. In this process, a flexible blade is used to directly meter the coating liquid onto a moving web from the fluid reservoir, or the blade can be combined with a roll-coating operation, as shown in Figure 11-10B. The blade is flexible and pressure developed under the blade determines the coating thickness.

The most direct method to apply a coating is by direct extrusion onto the moving web, as shown in Figure 11-10C. This process is sometimes called *curtain coating* and is often used in conjunction with UV curing. The thickness of the coating is determined by the speed of the web and the volumetric output of the extruder.

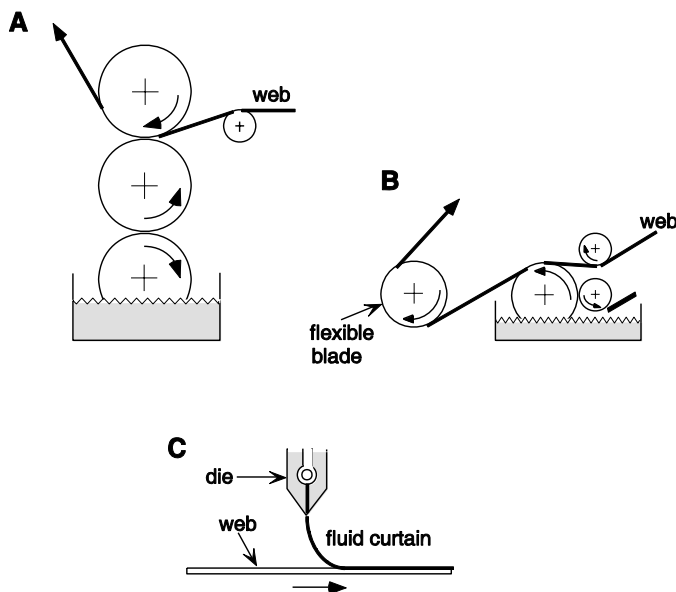


Figure 11-10 Examples of coating process. **A.** Roll coating. **B.** Blade coating. **C.** Curtain coating. After S. Middleman, *Fundamentals of Polymer Processing*. 1977, New York: McGraw-Hill. Reproduced with permission of the author.

11.2 Introduction to Polymer Rheology

The viscous flow of a Newtonian fluid is described by *Newton's law of viscosity* given for shear flow as

$$\boxed{\tau = \mu \frac{d\gamma}{dt}} \quad (11.1)$$

where τ is shear stress, μ is the Newtonian viscosity coefficient, and γ is the shear strain. The time dependence of shear strain is called the *shear strain rate* or simply shear rate:

$$\boxed{\dot{\gamma} = \frac{d\gamma}{dt}}. \quad (11.2)$$

A *simple flow* is defined as one in which *only one* of the three components of the velocity vector

$$\mathbf{u} = (u_1, u_2, u_3) \quad (11.3)$$

is nonzero. The subscripts 1, 2, and 3 identifying the three components of the velocity vector, u_i , refer to the axes of the particular coordinate system used to analyze the flow process (i.e., x , y , and z in rectangular coordinates; r , θ , and z in cylindrical coordinates; and r , θ , and ϕ in spherical coordinates).

An example of a simple shear flow is Couette shear flow between two infinitely wide parallel plates, as illustrated in Figure 11-11. To analyze this simple flow, it is convenient to establish a rectangular-coordinate system having its x -axis fixed in the bottom plate and oriented along the shear direction, with the y -axis perpendicular to the plate surface. In this case, the shear strain, γ , is defined as the ratio of the deformation of a differential element in the x -direction (dx) to that in the y -direction (dy) during shear. It is easily shown that the shear rate in plane Couette flow is equal to the velocity gradient as

$$\dot{\gamma} = \frac{d\gamma}{dt} = \frac{d}{dt} \left(\frac{dx}{dy} \right) = \frac{d}{dy} \left(\frac{dx}{dt} \right) = \frac{du_x}{dy} \quad (11.4)$$

where u_x is the velocity of the fluid in the x -direction. The *maximum* shear rate occurs at the moving plate surface and is given as U/H , where U is the constant (maximum) velocity of the upper plate moving in the x -direction and H is the distance of separation between the two plates. The *minimum* shear rate is zero, which occurs at the bottom (stationary) plate (i.e., $y = 0$) assuming there is *no slip* of the fluid layer at the plate surface; therefore, $u_x(0) = 0$.

As illustrated in Figure 11-11 and later discussed in Section 11.3.2, the velocity, u_x , is a linear function of the y -coordinate. In the case of Newtonian fluids such as water and mineral oil, the viscosity, μ , is a function of temperature and pressure but is *independent* of $\dot{\gamma}$. In contrast, the viscosity of non-Newtonian fluids such as concentrated polymer solutions and polymer melts is a function of temperature, pressure, and $\dot{\gamma}$. In addition, the viscosity of polymer solutions and melts exhibits a

strong dependence on molecular weight. These unique aspects of polymer rheology are discussed in the following section.

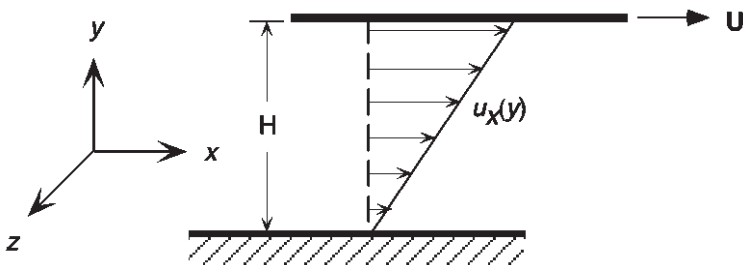


Figure 11-11 Representation of simple shear flow (plane Couette flow) between parallel plates whereby the upper plate is moving at a constant velocity (U).

11.2.1 Non-Newtonian Flow

Shear-Rate Dependence. The non-Newtonian or *apparent viscosity*, η , of polymer solutions and melts is defined following Newton's law of viscosity (eq. (11.1)) as

$$\boxed{\tau = \eta(\dot{\gamma})\dot{\gamma}}. \quad (11.5)$$

Equation (11.5) is called the *generalized Newtonian fluid* (GNF) model. The actual analytical relationship between τ and $\dot{\gamma}$ and, therefore, the dependence of η on $\dot{\gamma}$ are given by the *constitutive* equation of the material. Melts of high-molecular-weight polymers and their concentrated solutions display three characteristic regions, as illustrated in Figure 11-12. At low shear rates, η is nearly independent of

* Since τ and $\dot{\gamma}$ are the shear stress and shear rate, respectively, the viscosity defined by eq. (11.5)

$$\eta = \frac{\tau}{\dot{\gamma}}$$

is the *shear* viscosity. An extensional or Trouton viscosity is defined by the corresponding expression for tensile stress and strain as

$$\eta_T = \frac{\sigma}{\dot{\epsilon}}.$$

The extensional viscosity and its dependence upon the tensile strain rate are important in modeling processing operations where significant extensional flow occurs, such as converging flow in a runner during injection molding and during calendering and blow-molding operations. Extensional viscosity may also have significant importance to the drag-reduction properties of dilute polymer solutions (see Section 11.2.6).

$\dot{\gamma}$ (i.e., Newtonian behavior) and approaches a limiting zero shear rate value of η_∞ . At higher $\dot{\gamma}$, η decreases with increasing $\dot{\gamma}$. Fluids that display this behavior are termed *shear thinning*. Finally, η once again approaches a limiting Newtonian plateau, η_0 , at very high $\dot{\gamma}$.

The molecular basis for shear-thinning behavior is the effect of shear on entanglements, as illustrated in Figure 11-13. At low shear rates, the entanglements impede shear flow and, therefore, viscosity is high. As the shear rate increases, chains begin to orient in the flow direction and disentangle from one another—the viscosity begins to drop. Finally, the molecules become fully oriented in the flow direction at very high shear rates. At this point, stable entanglements are no longer possible and the viscosity reaches a low level that is again independent of shear strain rate. This second Newtonian plateau region is observed in the case of polymer solutions but is rarely observed for polymer melts because the shear rates required for chain orientation in the melt are so high that the chains actually can be broken (i.e., shear-induced degradation or mechanodegradation; see Section 6.1.5). In rare cases, viscosity may *increase* with increasing shear rate. Fluids that exhibit this behavior are called *shear thickening* (or *dilatant*). Examples of shear-thickening behavior are generally limited to concentrated suspensions such as PVC pastes and polymer melts that undergo shear-induced crystallization.

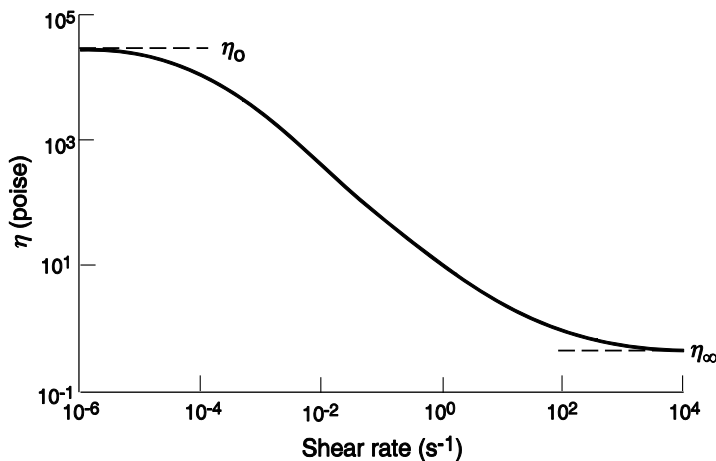


Figure 11-12 Typical dependence of apparent viscosity, η , of a polymeric melt on shear rate, $\dot{\gamma}$, showing the zero-shear viscosity, η_0 , plateau. Adapted from H. A. Barnes, J. F. Hutton, and K. Walters, *An Introduction to Rheology*. 1989, Elsevier Science. Copyright 1989, Elsevier Science.

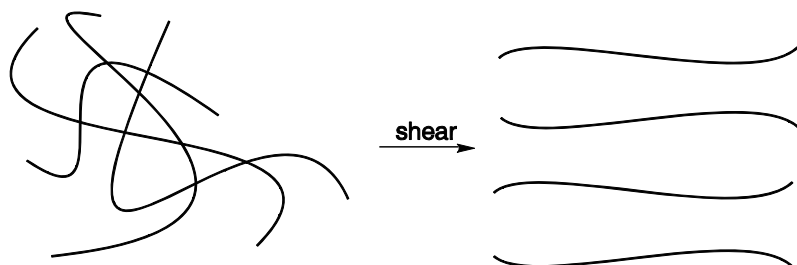


Figure 11-13 Idealized view of the effect of shear on the entanglements of melts and concentrated polymer solutions.

Molecular-Weight Dependence. The significance of entanglements to shear-thinning flow suggests that molecular weight and the critical molecular weight for entanglements, M_c (see Section 4.1.1), should significantly influence the rheological properties of polymers. It has been shown that the zero-shear viscosity, η_0 , is directly related to the weight-average molecular weight, \bar{M}_w , when $\bar{M}_w < M_c$ but follows a 3.4 power dependence on \bar{M}_w when $\bar{M}_w \geq M_c$. In addition, the onset of shear-thinning behavior occurs at progressively lower $\dot{\gamma}$ as molecular weight increases, as shown by viscosity data for polystyrene ($M_c = 31,200$) given in Figure 11-14.

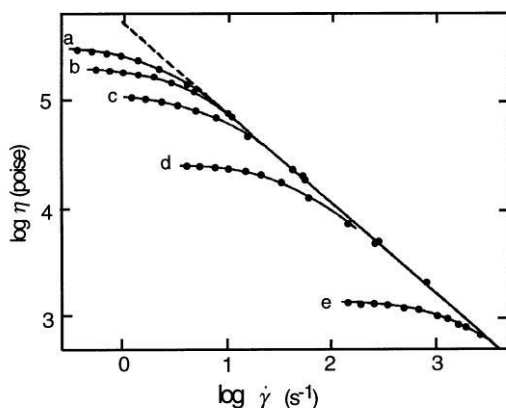


Figure 11-14 Effect of increasing molecular weight on the dependence of polymer viscosity on $\dot{\gamma}$ for polystyrene at 183°C. Molecular weights: (a) 242,000; (b) 217,000; (c) 179,000; (d) 117,000; and (e) 48,500. Adapted from R. A. Stratton, *The Dependence of Non-Newtonian Viscosity on Molecular Weight for "Monodisperse" Polystyrene*. Journal of Colloid and Interface Science, 22: p. 517–530. Copyright 1966, with permission from Elsevier Science.

Temperature Dependence. The temperature dependence of the apparent viscosity of a polymer melt follows a typical *Arrhenius relationship* at high temperatures, ca. 100°C above T_g , as given by

$$\boxed{\eta = \eta_r \exp \left[\frac{E}{R} \left(\frac{1}{T} - \frac{1}{T_r} \right) \right]} \quad (11.6)$$

where η_r is the viscosity at some reference temperature, T_r , E is the activation energy (typically 21 to 210 kJ mol⁻¹), and R is the ideal gas constant. At lower temperatures, in the vicinity of the glass-transition temperature, approximately $T_g < T < T_g + 100^\circ\text{C}$, viscosity increases much more rapidly with decreasing temperature than is given by the Arrhenius expression. In this case, the temperature dependence of melt viscosity can be obtained by the WLF equation (see Section 5.1.6) as

$$\log \left[\frac{\eta(T)}{\eta(T_g)} \right] = \log a_T = \frac{-C_1(T - T_g)}{C_2 + T - T_g} \quad (11.7)$$

where $\eta(T_g)$ is the viscosity at T_g . Figure 11-15 shows the fit of experimental data for polycarbonate, for which excellent agreement between experimental viscosities and those predicted by the WLF equation is observed over the temperature range from $T_g + 55^\circ\text{C}$ to $T_g + 185^\circ\text{C}$ [2].

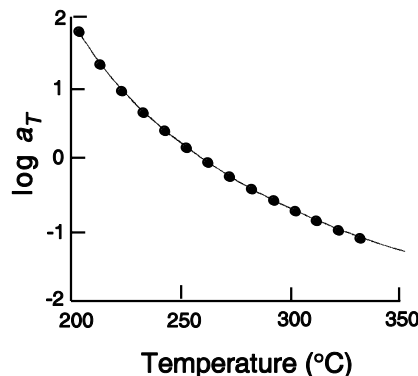


Figure 11-15 WLF fit (curve) of the shift factor, $a_T = \eta(T)/\eta(260^\circ\text{C})$, for polycarbonate at a reference temperature of 260°C. Adapted from P. Lomellini, *Viscosity-Temperature Relationships of a Polycarbonate Melt: Williams—Landel—Ferry versus Arrhenius Behaviour*. Makromolekulare Chemie, 1992. **193**: p. 6979, with permission of the publisher.

As discussed in Chapter 4, one view of the glass transition is that it is an iso-viscous state where the viscosity at T_g , $\eta(T_g)$, is approximately 10^{12} Pa-s (10^{13} poise) [3]. Use of eq. (11.7) provides a means of relating the WLF parameters, C_1 and C_2 , to the free volume, V_f , and the thermal-expansion coefficient, α , of the polymer as shown in Appendix A.1 of this chapter.

Pressure Dependence. Unlike the case for the glass-transition temperature, viscosity can be significantly affected by pressure. This pressure dependence may be an important consideration in the design of some processing operations, such as injection molding for which mold pressures can be very high. At constant temperature, the effect of pressure on viscosity can be approximated by the relation

$$\ln\left(\frac{\eta}{\eta_r}\right) = \beta(p - p_r) \quad (11.8)$$

where η_r is a reference viscosity corresponding to some reference pressure, p_r , and β is a pressure coefficient in the range of 0.87 to 4.93×10^{-8} Pa⁻¹ (0.6 to 3.4×10^{-4} psia⁻¹). As an example, the viscosity of a polystyrene melt at 250°C will nearly double with an increase in pressure from 13.8 to 27.6 MPa (2000 to 4000 psi). Often, in the modeling of processing operations, it is necessary to neglect the effect of pressure in order to obtain analytical or even numerical solutions that are manageable, as discussed in Section 11.3.

Time Dependence. Shear-thinning (and shear-thickening) behavior is considered to be reversible providing no thermal or mechanical degradation has occurred. In some cases, the subsequent flow behavior of a previously sheared fluid may depend upon the prior shear history and the time allowed for recovery. A fluid whose viscosity is reduced by prior deformation or decreases with time under conditions of constant stress or shear rate is called *thixotropic* [4]. Eventually, the viscosity will recover (increase) once the stress is removed. An example of a thixotropic fluid is non-drip latex paint. Similarly, a fluid whose viscosity has increased as a result of prior deformation history or increased in time under application of constant stress or strain is called antithixotropic. As will be shown shortly, the successful modeling of polymer-processing operations is difficult enough without introducing time-dependent viscosity terms, and no attempt to do so will be made here.

11.2.2 Viscosity of Polymer Solutions and Suspensions

Solution Viscosity. For very dilute solutions, polymer coils are widely separated and do not overlap, as illustrated in Figure 11-16. At a critical concentration, c^{**} , marking the transition from the extremely dilute to dilute regions, the hydrodynamic volumes of individual coils start to touch. As concentration is further increased ($c >$

c^*), coils begin to overlap and finally entanglements are formed that increase viscosity.

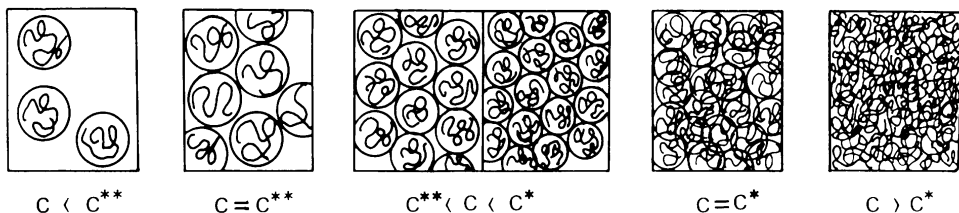


Figure 11-16 Critical concentration regions showing transition from the extremely dilute region ($c < c^{**}$) where polymer coils are isolated to the dilute region ($c > c^*$) where coils become entangled. Reproduced from A. Dondos and C. Tsitsilianis, *Viscoelastic Study of Extremely Dilute Macromolecular Solutions: Critical Concentration c and the Intrinsic Viscosity of the Polystyrene through Scaling Laws. The Value of the Huggins Constant*, Polymer International, 1992. **28**: p. 151–156. Copyright Society of Chemical Industry. Reproduced with permission. Permission is granted by John Wiley & Sons Ltd. on behalf of the SCI.

The critical concentration, c^* , may be marked by an abrupt increase in the relative viscosity increment* (eq. 3.104). This transition is shown for cellulose acetate (CA) in dimethyl sulfoxide (DMSO) in Figure 11-17. The critical transition concentration was found to be 3.7 g dL^{-1} and approximately independent of the solvent^[5], although a dependence of c^* on the molecular weight of CA would be expected.

* The relative viscosity increment is also known as the specific viscosity, η_{sp} .

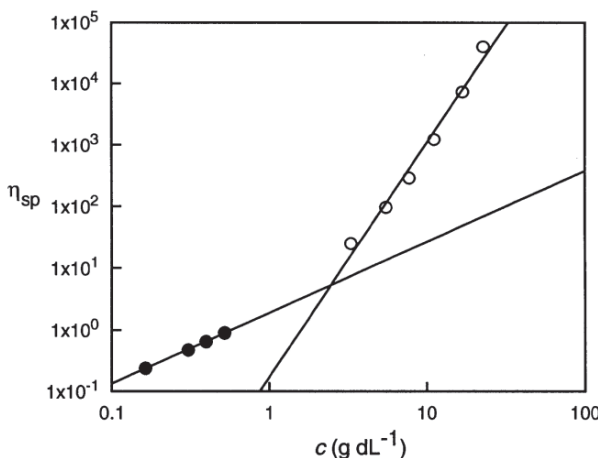


Figure 11-17 Concentration dependence of the specific viscosity, η_{sp} of dilute and moderately concentrated solutions of cellulose acetate in dimethyl sulfoxide [5]. The intersection of straight lines that are drawn through the dilute-solution (●) and concentrated-solution (○) data marks the critical concentration, c^* (ca. 3.7 g dL⁻¹ in this case).

Below c^* , viscosity is proportional to concentration, but above c^* , viscosity is approximately proportional to the *fifth power* of concentration. In general, the effect of molecular weight and solution concentration of viscosity can be modeled as [6]

$$\eta = K(c\rho)^\alpha M^\beta \quad (11.9)$$

where K is a constant and α and β are parameters; the ratio β/α is usually in the range from 0.54 to 0.74.

The presence of a solvent (or plasticizer) has two effects on polymer viscosity in the concentrated solution region: the solvent (1) lowers the T_g and (2) increases the molecular weight between entanglements, M_e (see Section 4.1.1), as

$$M_e = \frac{M_e^0}{\phi} \quad (11.10)$$

where M_e^0 is the molecular weight between entanglements for the undiluted polymer and ϕ is the volume fraction of solvent. As polymer concentration increases, polymer solutions become more non-Newtonian as the number of entanglements increases, as illustrated for concentrated solutions of polystyrene in *n*-butyl benzene in Figure 11-18. The data show that viscosity of a concentrated polymer solution rapidly increases with increasing polymer concentration. In addition, the onset of shear-thinning behavior occurs at lower shear rate with increasing concentration.

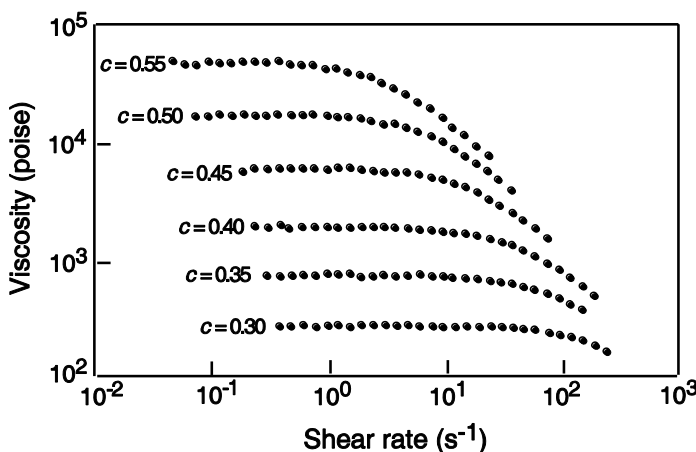


Figure 11-18 Viscosity of polystyrene (411,000 molecular weight) in *n*-butyl benzene at different concentrations (c , units of g cm^{-3}) as a function of shear strain-rate ($\dot{\gamma}$) at 30°C . Adapted from W. W. Graessley, R. L. Hazleton, and L. R. Lindeman, *The Shear-Rate Dependence of Viscosity in Concentrated Solutions of Narrow-Distribution Polystyrene*, Transactions of the Society of Rheology, 1967, 11: p. 267–285 (1967), with permission of the publisher.

Viscosity of Suspensions. In many cases, concentrated polymer solutions and melts may contain particulate or fiber fillers. For example, commercial rubber formulations usually contain carbon black. Poly(vinyl chloride) for floor tile or wire insulation applications typically contains rigid fillers such as calcium carbonate. A *plastisol* is a suspension of polymer particles in a liquid plasticizer, while a *latex* is a suspension of polymer particles in water. In all these cases, suspended particles affect the rheological properties of the suspension.

In 1906, Einstein theorized that the viscosity of dilute suspensions in a Newtonian liquid can be expressed as

$$\eta = \eta^\circ (1 + k_E \phi) \quad (11.11)$$

where η° is the viscosity of the suspending liquid, k_E is called the Einstein coefficient, and ϕ is the volume fraction of suspended particles. The Einstein coefficient depends upon the geometry of the dispersed phase as well as the orientation of fibers and other nonspherical fillers. In the case of spherical fillers, such as calcium carbonate, k_E is 2.5. Equation (11.11) indicates that the relative viscosity, η/η° , depends only upon the concentration of filler and is independent of the size and nature of the particles. Over the years, many other equations have been proposed with various degrees of success. One of the best, proposed by Mooney, is given as

$$\ln\left(\eta/\eta^{\circ}\right) = \frac{k_E\phi}{1-\phi/\phi_m} \quad (11.12)$$

where ϕ_m is the maximum packing (volume) fraction, which varies from 0.065 for rod-shaped particles to 0.7405 for hexagonal close-packed spheres. It may be noted that even Newtonian fluids such as water become non-Newtonian at moderate concentrations of suspended particles. Some suspensions such as lattices and plastisols exhibit yield (Bingham) behavior, as discussed in the following section.

11.2.3 Constitutive Equations

In order to model a simple-flow geometry as a prelude to handling more complicated processes such as extrusion, it is necessary to begin with some reasonable model for the relation between shear stress and shear rate (eq. (11.5)). The most widely used relationship is the *power-law* (or Ostwald–de Waele–Nutting) model given as

$$\boxed{\tau = m\dot{\gamma}^n} \quad (11.13)$$

where m is called the *consistency* and n is the *power-law index*. For a given polymer, m is a decreasing function while n is an increasing function of increasing temperature, which means that the melt becomes more Newtonian (i.e., less shear thinning) with an increase in temperature. It follows from the GNF model given by eq. (11.5) that the dependence of apparent viscosity, η , on $\dot{\gamma}$ for a power-law fluid (PLF) is

$$\boxed{\eta = m\dot{\gamma}^{n-1}}. \quad (11.14)$$

Equation (11.14) indicates that, when $n = 1$, η is independent of $\dot{\gamma}$. This means that Newton's law of viscosity may be considered to be a special case (i.e., $n = 1$ and $m = \mu$) of the more general PLF model. For shear-thinning behavior, $n < 1$. Representative values of the power-law parameters, m and n , and the $\dot{\gamma}$ range for which they are applicable are given for several commercially important polymers in Table 11-1. Some non-Newtonian fluids require an application of a threshold (or yield) stress, τ_y , before flow will begin. Such fluids are termed *Bingham* fluids and may be viewed as having some internal structure that collapses at τ_y . Examples include some suspensions, slurries, pulps, and ketchup. If the viscous response is Newtonian once the yield stress has been reached, the constitutive equation for a Bingham fluid can be written as

$$\tau = \tau_y + \mu\dot{\gamma}. \quad (11.15)$$

Table 11-1 Power-Law Parameters for Some Representative Polymers

Polymer	T (°C)	$\dot{\gamma}$ Range (s^{-1})	m (N s ⁿ m ⁻²)	n
Polycarbonate	180	100–1000	8.39×10^3	0.64
	200	100–1000	4.31×10^3	0.67
	220	100–1000	1.08×10^3	0.80
Polypropylene	180	100–400	6.79×10^3	0.37
	190	100–3500	4.89×10^3	0.41
	200	100–4000	4.35×10^3	0.41
Polystyrene	190	100–4500	4.47×10^4	0.22
	210	100–4500	2.38×10^4	0.25
	225	100–5000	1.56×10^4	0.28

It is clear that eq. (11.14) is suitable for representing the dependence of viscosity on shear rate only in the shear-thinning region where a plot of $\log \eta$ versus $\log \dot{\gamma}$ is linear. Since this is normally the $\dot{\gamma}$ range for most important processing operations, particularly extrusion and injection molding (see Table 11-2), this restriction is seldom significant considering the simplicity of the model. Other constitutive equations, such as the Carreau model [7], are available to fit data over a more extensive $\dot{\gamma}$ range but, typically, make the solution to processing problems more difficult.

Table 11-2 Typical $\dot{\gamma}$ Range for Polymer Processing Operations

Operation	$\dot{\gamma}$ Range (s^{-1})
Compression molding	1–10
Calendering	$10\text{--}10^2$
Extrusion	$10^2\text{--}10^3$
Injection molding	$10^3\text{--}10^4$

11.2.4 Elastic Properties of Polymeric Fluids

A unique and important characteristic of polymer melts and concentrated solutions is their elastic recovery after shear deformation. When polymer chains are oriented in the flow direction, there is an entropic driving force for the chains to recover their random coil conformation upon cessation of the stress. For example, chains undergoing shear deformation during flow in a capillary will recover their original equilibrium conformations at the exit of a capillary where stress goes to zero. This gives rise to *die swell* whereby the diameter of the extruded fiber is larger than the diameter of the capillary. As an illustration, the die swell of polyethylene extruded through a capillary die is shown in Figure 11-19.

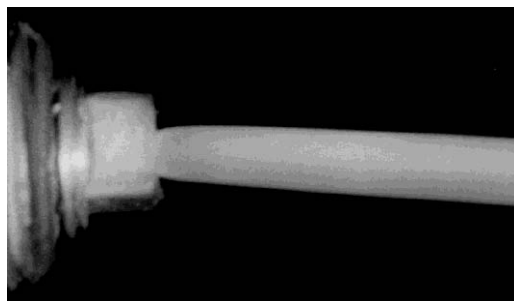


Figure 11-19 Die swell of high-density polyethylene exiting a circular tube at 180°C. Reprinted from C. D. Han, *Rheology in Polymer Processing*. 1976, New York: Academic Press. p. 3. Copyright 1976 Academic Press.

Quantitatively, elastic response is expressed in terms of *normal stresses*. Both stress and strain are second-order tensors and can be represented by a 3×3 matrix having nine components. For example, the stress tensor, τ , in an arbitrary coordinate system with axes 1, 2, and 3 (equivalent to x , y , and z in rectangular coordinates; r , z , and θ in cylindrical coordinates; or r , θ , and ϕ in spherical coordinates) is given as

$$\boldsymbol{\tau} = \begin{pmatrix} \tau_{11} & \tau_{12} & \tau_{13} \\ \tau_{21} & \tau_{22} & \tau_{23} \\ \tau_{31} & \tau_{32} & \tau_{33} \end{pmatrix}. \quad (11.16)$$

The first and second subscripts of each stress component, τ_{ij} , in the matrix identify the row (the direction of the force vector) and the column (the normal to the plane on which the component of force acts), respectively. The stress tensor (as well as the strain tensor,* which can be written in an analogous fashion) is symmetrical. This means that $\tau_{ij} \equiv \tau_{ji}$ and, therefore, only six of the total of nine stress components are independent. The normal stress components are those lying along the diagonal of the matrix where $i \equiv j$ (i.e., τ_{11} , τ_{22} , τ_{33}). The orientation of normal stresses for a cubical fluid element in simple plane shear is illustrated in Figure 11-20.

* The rate-of-deformation tensor is given as

$$\boldsymbol{\Delta} = \begin{pmatrix} \Delta_{11} & \Delta_{12} & \Delta_{13} \\ \Delta_{21} & \Delta_{22} & \Delta_{23} \\ \Delta_{31} & \Delta_{32} & \Delta_{33} \end{pmatrix}$$

for which the components of the tensor are symmetric, $\Delta_{ij} \equiv \Delta_{ji}$.

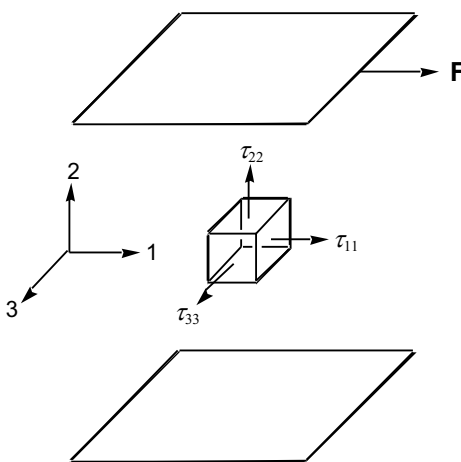


Figure 11-20 Normal stresses generated at the faces of a cubical element of fluid undergoing simple shear (shear stress τ_{12}).

When considering normal stresses, it is convenient to define two *normal-stress differences* that, like apparent viscosity, are functions of $\dot{\gamma}$. These are the *first* (or primary) *normal-stress difference*

$$\tau_{11} - \tau_{22} = \Psi_1(\dot{\gamma})\dot{\gamma}^2 \quad (11.17)$$

and the *second normal-stress difference*

$$\tau_{22} - \tau_{33} = \Psi_2(\dot{\gamma})\dot{\gamma}^2 \quad (11.18)$$

where Ψ_1 and Ψ_2 are called the first and second normal-stress coefficients, respectively, which are also functions of $\dot{\gamma}$. The apparent viscosity, η , and the two normal-stress coefficients are the three *material functions* that describe the complete shear response (viscous and elastic) of polymeric fluids.

In terms of their importance to polymer processing, the first normal-stress difference is the more significant of the two. It is responsible for the swelling of extrudate exiting a die (called *die swell*, the Barus effect, or *puffup*) and for a nonzero pressure drop that has been observed to occur at the die exit (see Section 11.4.1). By comparison, the second normal-stress difference is small (only 10% to 15% of the magnitude of the first normal-stress difference) and has a negative sign. Both normal-stress differences can be measured directly at low $\dot{\gamma}$ by modern rheological instruments such as cone-and-plate and parallel-plate rheometers, which have sensitive force transducers mounted in the three directions orthogonal to the plane of shear. Basic concepts of rheometry are covered in Section 11.4. For evaluation of normal-stress effects at higher $\dot{\gamma}$ typical of actual processing operations, online rheometers such as a slit die (rectangular die) attached to an extruder may be used.

By reading pressures along the length of the die using flush-mounted pressure transducers, the exit pressure may be determined by extrapolation of a plot of pressure versus die length. Correlations may then be used to relate die swell to exit pressure for given operating conditions.

11.2.5 Melt Instabilities

It has been widely recognized that polymer extrudates of a wide variety of shapes including tubing, rods, and other profiles can develop distortions at some critical shear flow rates. This general phenomenon of distorted extrudates is called *melt fracture*. Distortions can take the form of bamboo, spirals, or “sharkskin” as shown in Figure 11-21. Although this behavior has been widely observed, the cause of sharkskin and other forms of melt fracture is still a controversial subject [8]. A recent explanation attributes sharkskin formation to chain disentanglement at the die wall in the exit region [9]. This may be due to a combination of interfacial slip and cohesive failure.

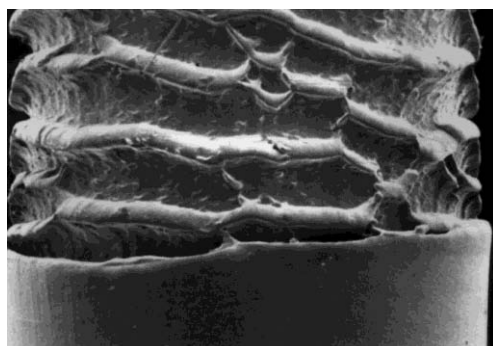


Figure 11-21 Scanning electron micrograph showing the onset of sharkskin in an extruded LLDPE rod (0.76 mm in diameter). Reproduced from M. M. Denn, *Pressure Drop Flow Rate Equation for Adiabatic Capillary Flow with a Pressure- and Temperature-Dependent Viscosity*. Polymer Engineering and Science, 1981. **21**: p. 65–68, by permission of the publisher.

11.2.6 Drag Reduction

It has been observed that dilute solutions (1 to 100 ppm) of many high-molecular-weight ($>100,000$) linear polymers can reduce turbulent friction in fluid flow by as much as 70% to 80%. This *drag reduction* was first observed in 1948 for flow in a circular pipe [10]. The most effective drag-reducing agents are flexible and high-

molecular-weight polymers. Poly(ethylene oxide) (PEO) is widely used as a drag-reducing polymer in aqueous solutions. Another water-soluble polymer that is effective as a drag-reducing agent is polyacrylamide. Some naturally occurring polymers such as guar and xanthan are also effective drag reducers. The *oil-soluble* polymer polyisobutylene (PIB) is effective for drag reduction of crude oil [11]. Suspensions of some fibers, including nylons, can also impart good drag reduction in turbulent flow.

Although the exact mechanism of drag reduction is still unclear, it is possible that drag reduction may be related to extensional flow. During flow, long polymer chains become disentangled and oriented in the direction of flow. Extensional viscosity (see Section 11.2.1) significantly increases and a form of strain-rate hardening occurs, which imposes a maximum limit on the strain rate. The high extensional viscosity reduces turbulent fluctuations (probably through the suppression of the roll-wave motion and vortex stretching in the sublayer) and, thereby, reduces friction.

Applications for drag reduction include those for which reduced friction in fluid flow is important. For example, a small amount of a water-soluble polymer can be injected into sewers during periods of heavy rain to upgrade flow and, thereby, prevent flooding. A drag-reducing polymer can also be injected at the bow of a ship to decrease friction and increase speed or be used to decrease pressure drop in water lines for firefighting.

11.3 Analysis of Simple Flows

Polymer-processing operations like extrusion, injection molding, pultrusion, roll coating, blow molding, and others are too complicated to model rigorously. Fortunately, most processing operations can be broken down into a set of simpler flow processes for which analytical or numerical solutions can be obtained using various simplifying approximations and constraints. In this way, it is possible to understand how process variables such as screw speed and temperature in an extruder affect performance variables such as volumetric output. A complete discussion of the modeling of polymer processes is well beyond the scope of this chapter and the reader is encouraged to consult the excellent texts by Han, McKelvey, Middleman, and Tadmor and Gogos that are cited in the Suggested Reading at the end of this chapter. In the next sections, a general development of this subject is given along with some important results to serve as an introduction to the subject.

All polymer-processing operations involve the flow of polymer solutions or melts under a pressure gradient, shear deformation, or both. Since concentrated polymer solutions and polymer melts are non-Newtonian fluids, it is necessary to know the exact relationship between stress and strain—the constitutive equation—

in order to analyze flow through even the simplest geometry. As mentioned earlier, the PLF model is the one most frequently used. The simplest geometries to model are those for which (1) edge effects can be neglected, (2) flow is isothermal, and (3) a coordinate system (rectangular, cylindrical, or spherical) can be selected such that there is only one nonzero component of the velocity vector (i.e., flow is viscometric). Examples include pressure flow through long capillaries and between infinitely wide parallel plates. Simple *shear* flows* include those created by long concentric cylinders of which one cylinder is rotating or moving along the axial direction and between infinitely wide parallel plates of which one is moving at a constant velocity and is parallel to the other.

The solution to a simple-flow model is usually in the form of an expression for velocity as a function of the coordinate parameter(s) of the system. For example, the velocity in the axial (z) direction (i.e., along the length of a capillary) is a function of the radial distance from the centerline, $u_z(r)$, as discussed in the following section. In cases where the flow is directed out of the system, as it is in pressure flow through a capillary, the velocity profile can be used to obtain an expression for the volumetric flow rate.

In general, any solution to a flow problem must satisfy the conservation of momentum (i.e., the dynamic equations), conservation of mass (i.e., the continuity equations), and conservation of energy (i.e., the energy equations). The solutions given in the following examples of pressure and shear flow are obtained with the assumptions that the flow is isothermal, laminar, fully developed, steady, and incompressible. In addition, it is assumed that all body forces such as gravity can be neglected. The imposition of isothermal conditions is an especially major constraint, especially since processing operations are seldom isothermal and the flow of viscous polymer melts results in the generation of heat (i.e., viscous dissipation). The advantage of the restraint of isothermal flow is that it removes the energy equations from consideration in the solution and, therefore, greatly simplifies the task.[†] Taken

* A simple shear flow is formally defined as one for which a coordinate system can be chosen such that there is a nonzero component of velocity in only one direction

$$\mathbf{u} = (u_1 \ 0 \ 0)$$

and the rate-of-deformation tensor is given as

$$\Delta = \dot{\gamma} \begin{pmatrix} 0 & 1 & 0 \\ 1 & 0 & 0 \\ 0 & 0 & 0 \end{pmatrix}$$

where $\dot{\gamma}$ is the shear rate (a scalar).

[†] The energy equation for an incompressible fluid is written in Cartesian coordinates as

$$\rho \hat{C}_p \left(\frac{\partial T}{\partial t} + u_j \frac{\partial T}{\partial x_j} \right) = \frac{\partial}{\partial x_j} \left(k \frac{\partial T}{\partial x_j} \right) + \tau_{ij} \frac{\partial u_i}{\partial x_j}$$

together, these assumptions mean that only *one* dynamic equation usually needs to be solved for a particular problem.

The dynamic equations for an *incompressible* fluid of density ρ subject to an external force field, \mathbf{f} , are written in Cartesian coordinates as

$$\boxed{\rho \left(\frac{\partial u_i}{\partial t} + u_j \frac{\partial u_i}{\partial x_j} \right) = \frac{\partial T_{ij}}{\partial x_j} + \rho f_i} \quad (11.19)$$

where u is velocity, t is time, f is a body force (e.g., gravity), and the summation is over all j —the coordinate parameters x , y , and z . This means that there are three dynamic equations for each coordinate system. The parameter T_{ij} appearing in eq. (11.19) is a component of the *total* stress tensor and is defined as

$$T_{ij} = \tau_{ij} - p\delta_{ij} \quad (11.20)$$

where τ_{ij} is the component of the shear-stress tensor (see eq. (11.16)) corresponding to T_{ij} and sometimes called the dynamic (or deviatoric) stress tensor; p is (hydrostatic) pressure; and δ_{ij} is called the Kronecker delta, a component of a unity tensor* (where $\delta_{ij} = 1$ for $i = j$ and $\delta_{ij} = 0$ for $i \neq j$).

The continuity equation for an incompressible fluid is written in Cartesian coordinates as

$$\frac{\partial u_i}{\partial x_i} = 0. \quad (11.21)$$

The complete expressions for the dynamic and continuity equations in Cartesian and cylindrical coordinates are given in Appendix A.2 at the end of this chapter.

Velocity is introduced into the solution of a process-flow problem through its relationship to strain (e.g., eq. (11.4)) and the constitutive equation (eq. (11.5)), which relates the stress, τ , and shear strain rate.[†] For simple isothermal flows, where

where \hat{C}_p is the heat capacity per unit mass and k is the thermal conductivity. The dynamic and energy equations are usually coupled through the velocity terms, making the solution of differential equations especially difficult. Numerical solutions are available for adiabatic conditions, but, in general, temperature effects are very difficult to handle for non-Newtonian flow.

* The unity tensor is formally given as

$$\boldsymbol{\delta} = \begin{pmatrix} 1 & 0 & 0 \\ 0 & 1 & 0 \\ 0 & 0 & 1 \end{pmatrix}.$$

[†] It should be noted that the well-known Navier–Stokes equations are just a special case of the more general dynamic equations—one for which the incompressible fluid is Newtonian and, therefore,

there is only one nonzero component of the velocity vector, the problem reduces to the solution of a single differential equation provided by the dynamic equations.

The terms within parentheses on the left-hand side of eq. (11.19) are called the *inertial* terms and usually can be neglected.* This is particularly fortunate since the second of the inertial terms introduces nonlinearity to the set of partial differential equations. Since we are also neglecting body forces, what remains of eq. (11.19) is a much simpler relationship:

$$\frac{\partial T_{ij}}{\partial x_{ij}} = 0. \quad (11.22)$$

Another assumption, and one that is very good, is that there is *no slip* between the fluid and the surface of the flow geometry. This no-slip assumption provides one or two boundary conditions for the solution of the differential equation. The example of pressure flow through a capillary given in the next section serves to illustrate this general approach for solving a fluid-flow problem.

11.3.1 Pressure (Poiseuille) Flow

Flow through a Capillary. Analysis of simple pressure flow through a tube or capillary is important in the modeling of extrusion through a capillary die and in the measurement of melt viscosity by means of a capillary rheometer, as discussed in Section 11.4.1. As discussed in the previous section, it is helpful to assume that flow is isothermal, fully developed, incompressible, laminar, and steady. For an infinitely long, horizontal tube for which undeveloped flow in the entrance region and gravitational forces can be ignored, the dynamic equations are reduced to the single differential equation (see Problem 11.8)

$$\frac{\partial p}{\partial z} = \frac{1}{r} \left[\frac{\partial}{\partial r} (r \tau_{rz}) \right] \quad (11.23)$$

where z is chosen to be the direction of flow (the axial direction). Substitution of the PLF constitutive equation (eq. (11.13)) in the form

$$\tau_{rz} = m \dot{\gamma}_{rz}^n = m \left(\frac{du_z}{dr} \right)^n \quad (11.24)$$

$$\tau_{ij} = \mu \dot{\gamma}_{ij}.$$

* Note that all derivatives with respect to time (e.g., the first of the inertial terms) become zero when the flow is assumed to be steady in time.

into eq. (11.23) and integration twice give the velocity of a PLF as

$$u_z(r) = \left(\frac{nR}{1+n} \right) \left(\frac{R\Delta p}{2mL} \right)^{1/n} \left[1 - \left(\frac{r}{R} \right)^{(1+n)/n} \right] \quad (11.25)$$

where R is the tube radius, $\Delta p/L$ is the pressure drop across the capillary per unit length, and r is the radial distance from the centerline (see Problem 11.9). Boundary conditions are obtained by realizing that the velocity at the surface (i.e., at $r = R$) of the capillary wall is zero, given a condition of no-slip, and the maximum velocity

$$u_z^{\max} = \left(\frac{nR}{1+n} \right) \left(\frac{R\Delta p}{2mL} \right)^{1/n} \quad (11.26)$$

occurs at the centerline ($r = 0$) and, therefore, $du_z/dr = 0$ (i.e., $\dot{\gamma} = 0$ at the centerline of the capillary). Division of eq. (11.25) by eq. (11.26) gives the velocity profile in dimensionless form as

$$\frac{u_z}{u_z^{\max}} = 1 - \left(\frac{r}{R} \right)^{(1+n)/n}. \quad (11.27)$$

As shown in Figure 11-22, the velocity profile of a PLF becomes flatter (i.e., more plug flow) with decreasing n (i.e., with increasing shear-thinning behavior).

The volumetric flow rate, Q , through the capillary can be obtained by integrating the velocity function (eq. (11.25)) as

$$Q = \int_{r=0}^R \pi r u_z(r) dr = \left(\frac{n\pi R^3}{1+3n} \right) \left(\frac{R\Delta p}{2mL} \right)^{1/n}. \quad (11.28)$$

For the special case of a Newtonian fluid for which $m = \mu$ and $n = 1$, eq. (11.28) reduces to the familiar *Hagen–Poiseuille equation*

$$Q = \frac{\pi R^4 \Delta p}{8\mu L}.$$

(11.29)

Similar models can be developed for isothermal pressure flow through other simple-flow geometries such as an annulus or infinitely wide parallel plates. Respectively, these approximate the flow through tubing (i.e., annular die) and sheet (i.e., slit) dies used in extrusion. The exact form of the relationship between Q and the pressure drop, Δp , is called the *die characteristic*. As will be discussed in Section 11.5.1, a *screw characteristic*, which relates the volumetric output of an extruder as a function of different variables such as the extruder screw speed and geometry, may be obtained by modeling extruder operation as combined pressure and shear flow in a rectangular duct. Simultaneous solution of the die and screw charac-

teristics gives the operating conditions of pressure and flow rate for the coupled operation of the extruder and die. For completeness, the die characteristics for a PLF in different die geometries are summarized in Table 11-3.

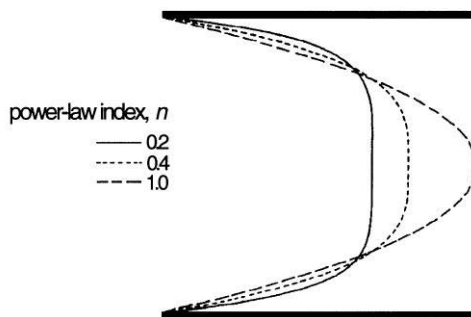


Figure 11-22 Velocity profile of a power-law fluid during isothermal pressure flow through a capillary as a function of the power-law index (n). Adapted from *An Introduction to Rheology*, H. A. Barnes, J. F. Hutton, and K. Walters, p. 34, Copyright 1989, with permission from Elsevier.

Table 11-3 Die Characteristics for a Power-Law Fluid in Pressure Flow

Geometry	Die Characteristic
Capillary	$Q = \left(\frac{n\pi R^3}{1+3n} \right) \left(\frac{R \Delta p}{2mL} \right)^{1/n}$
Annulus ^a	$Q = \left(\frac{n\pi R_o}{1+2n} \right) (R_o - R_i)^{2+1/n} \left(\frac{\Delta p}{2mL} \right)^{1/n} F(n, \kappa)$
Parallel plates ^b	$\frac{Q}{W} = \left[\frac{nH^2}{2(1+2n)} \right] \left(\frac{H \Delta p}{2mL} \right)^{1/n}$
Rectangular duct ^c	$Q = WH^2 \left(\frac{W \Delta p}{2mL} \right)^{1/n} S_p$

^a R_i , inner radius; R_o , outer radius; F is a function of n and the aspect ratio of the annulus, $\kappa = R_i/R_o$.

^b Infinitely wide parallel plates where H represents the separation of plates and W is unit width.

^c This is an example of a non-simple flow geometry; S_p is a shape factor that is a function of n and the aspect ratio, W/H .

11.3.2 Drag Flow

Plane Couette Flow. An example of a simple shear flow is plane (Couette) flow between two infinitely wide parallel plates as used as an example in Section 11.2 and illustrated in Figure 11-11. In this case, the top plate is driven at a constant velocity, U , in the x -direction while the bottom plate is fixed. Since the plates are infinitely wide, there are no edge effects and, therefore, the only nonzero component of the velocity vector is the x -component. This is an example of a *viscometric flow* as were the previous cases for simple pressure flows. Assuming that there is *no slip* of the fluid at the surface of the two plates and the vertical distance between the two plates is given as H , the velocity of the fluid element, u_x , at the top surface (i.e., $y = H$) is U , while the velocity at the bottom plate (i.e., $y = 0$) is zero. With these boundary conditions, the velocity profile is linear and *independent of the fluid type* (or constitutive equation). Specifically, the solution of the (x -component) dynamic equation gives the velocity of each fluid element as

$$u_x = \left(\frac{y}{H} \right) U. \quad (11.30)$$

The volumetric flow rate, Q , per unit width is then obtained from the velocity equation as

$$\frac{Q}{W} = \int_0^H u_x dy = \frac{UH}{2}. \quad (11.31)$$

As was the case for the velocity profile, the volumetric flow rate is independent of the fluid constitutive relationship—it is the same whether the fluid is Newtonian or a PLF.

Axial Annular Couette Flow. An important geometry that can be used as a model of a processing operation (e.g., wire coating as illustrated in Section 11.5.2) consists of two concentric cylinders of which the inner cylinder (e.g., the wire) is pulled at a constant linear velocity, U , as illustrated in Figure 11-23.

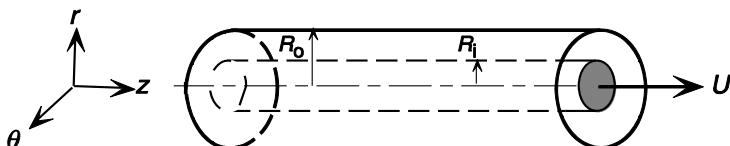


Figure 11-23 Representation of axial annular Couette flow. The inner cylinder is pulled at a velocity, U .

A solution of this problem for a Newtonian fluid is easily obtained and gives

$$\frac{u_z}{U} = \frac{\ln(r/R_o)}{\ln\kappa} \quad (11.32)$$

where $\kappa = R_i/R_o$. The solution for a PLF is given as^{*}

$$\frac{u_z}{U} = \frac{1}{\kappa^q - 1} \left[\left(\frac{r}{R_o} \right)^q - 1 \right] \quad (11.33)$$

where

$$q = 1 - \frac{1}{n}. \quad (11.34)$$

The volumetric flow rate is then obtained as

$$Q = 2\pi \int_{R_i}^{R_o} r u_z(r) dr. \quad (11.35)$$

Using eq. (11.33) and performing the integration give the following relationship for Q (in dimensionless form) of a power-law fluid in axial annular Couette flow:

$$\frac{Q}{2\pi R_o(R_o - R_i)U} = \frac{1}{q+2} \frac{1 - \kappa^{q+2}}{(1-\kappa)(\kappa^1 - 1)} - \frac{1 + \kappa}{2(\kappa^q - 1)}. \quad (11.36)$$

In this case, Q has the general significance of the volume of coating extruded on the wire per unit time. The complete analysis of an actual wire-coating operation is more complicated than indicated above because it involves the superposition of a pressure flow on the drag flow. The pressure flow is introduced as a result of the attachment of an extruder to the wire-coating die.

11.4 Rheometry

The relationship between stress and shear rate, and therefore the dependence of apparent viscosity upon shear rate, can be determined over a wide temperature range by a variety of techniques that utilize some of the simple pressure or shear geometries discussed in the previous section. These include capillary and Couette rheome-

^{*} In the case of axial annular Couette flow, the solutions for u_z and Q for a Newtonian fluid cannot be obtained from the PLF results by letting $n = 1$ ($q = 0$) and must be obtained independently.

try, which are based upon simple pressure flow through a capillary and simple shear flow through two rotating, concentric cylinders, respectively. Other common methods include cone-and-plate and parallel-plate rheometry, which can also give information concerning normal stresses through measurements by force transducers mounted in the direction normal to the plane of shear. Slit rheometers, which can be used to measure exit pressures in pressure flow through a rectangular channel, can be used to measure normal stress under typical processing conditions. The basics of capillary, Couette, and cone-and-plate rheometry are presented in this section. A complete discussion of rheometry can be found in a number of excellent texts such as those by Nielsen, Middleman, and Walters cited in the Suggested Reading at the end of this chapter.

11.4.1 Capillary Rheometer

In addition to providing a model for flow of a non-Newtonian fluid through a capillary die, an understanding of pressure flow through a tube may be used to determine the apparent viscosity of a polymer melt as a function of $\dot{\gamma}$. This method is called *capillary rheometry* and can be used over the $\dot{\gamma}$ range from 1 to 10^5 s^{-1} , which includes most polymer-processing operations (see Table 11-2). As can be shown by a simple force balance on a fluid element in the capillary, the shear stress ($\tau_{rz} \equiv \tau_{zx}$) given as

$$\tau = \frac{r\Delta p}{2L} \quad (11.37)$$

depends only upon the pressure drop and distance from the centerline—it is totally independent of whether the fluid is Newtonian or non-Newtonian (see Problem 11.6).

The experimental procedure requires the measurement of Q as a function of Δp through a capillary of known dimensions. The capillary is attached to a reservoir containing the polymer solution or melt, as illustrated in Figure 11-24. Pressurization of the reservoir forces the fluid through the capillary. From the value of Δp , the shear stress at the tube wall, τ_w (the maximum stress in capillary flow), is calculated as

$$\tau_w = \frac{R\Delta p}{2L}. \quad (11.38)$$

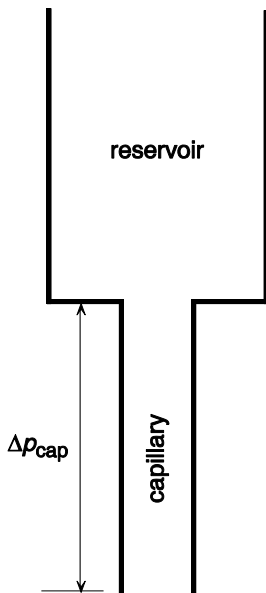


Figure 11-24 Pressure reservoir and capillary showing the overall pressure drop across the capillary (Δp_{cap}).

A second parameter used in the analysis of capillary-rheometry data is the *apparent shear rate*, $\dot{\phi}$, which is calculated from the experimentally measured volumetric flow rate, Q , as

$$\dot{\phi} = \frac{4Q}{\pi R^3}. \quad (11.39)$$

As in the case for τ_w , $\dot{\phi}$ is independent of the constitutive relation of the fluid; however, the exact form of the relationship between $\dot{\phi}$ and $\dot{\gamma}$ is dependent upon the fluid model. For example, $\dot{\gamma}_w \equiv \dot{\phi}$ for a Newtonian fluid. In the case of a PLF, it may be shown that the shear rate at the wall is given as

$$\dot{\gamma}_w = \frac{3n+1}{4n} \dot{\phi}. \quad (11.40)$$

The apparent viscosity for any non-Newtonian fluid is then calculated from values of the model-independent expression for τ_w (eq. (11.38)) and the model-dependent expression for $\dot{\gamma}$ (e.g., eq. (11.40)) through the GNF model (eq. (11.5)) as

$$\eta = \frac{\tau_w}{\dot{\gamma}_w}. \quad (11.41)$$

If the fluid behavior is power law over the entire experimental range of $\dot{\gamma}$, a plot of $\log \tau_w$ versus $\log \phi$ will be linear with slope equal to the power-law index, n , and an intercept of $\log m'$, which is related to the consistency, m , as^{*}

$$m = m' \left(\frac{4n}{3n+1} \right)^n. \quad (11.42)$$

Values of $\dot{\gamma}$ for each ϕ can then be calculated from knowledge of n and use of eq. (11.40).

One problem with the use of capillary rheometry is that the equations given above were obtained by assuming the usual model conditions: that the flow in the capillary is isothermal, fully developed, incompressible, laminar, and steady. The most difficult assumption to realize (and the one that is most easy to accommodate) is that the flow is fully developed over the entire length of the capillary. As shown in Figure 11-25, a significant pressure drop can occur at the entrance region of the capillary due to the extra stress needed to support the non-axial components of the velocity profile that result from the flow of the fluid from the large-diameter reservoir into the narrow capillary. For this reason, the pressure drop is not linear over the entire length of the capillary. Entrance effects can usually be neglected if the capillary is sufficiently long (e.g., $L/D > 200$); however, capillaries used in melt rheometry are typically short and, therefore, the experimental data need to be corrected for any entrance effects.

* It follows from eq. (11.24) in the form $\tau_w = m \dot{\gamma}_w^n$ and from eq. (11.40) that $\log \tau_w = n \log \phi + \log m'$.

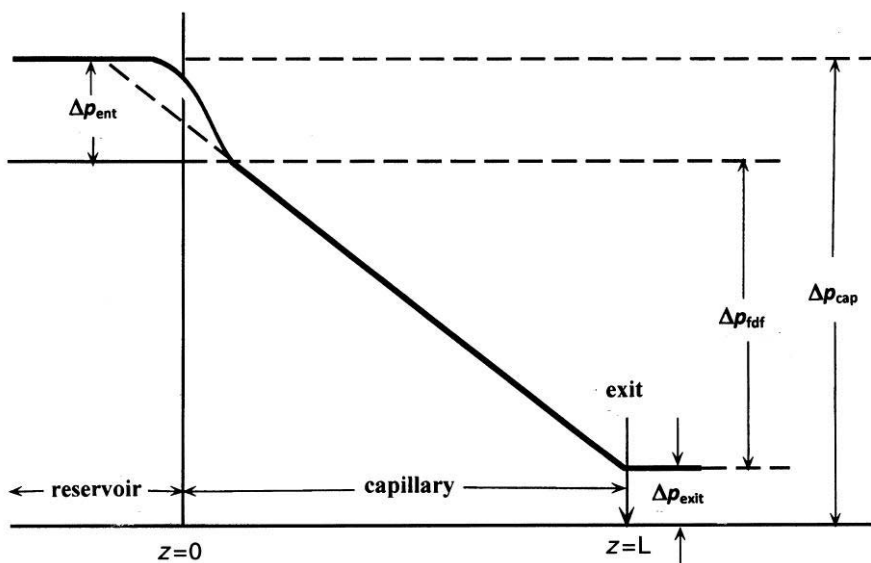


Figure 11-25 Pressure profile in reservoir and capillary (see Figure 11-23) showing the pressure drop in the entrance region between the reservoir and capillary, Δp_{ent} , the pressure drop across the capillary, and the exit pressure, p_{exit} .

Bagley [12] has suggested that entrance effects can be handled by assuming that the *effective* length of the capillary is greater than the actual length and, therefore, the shear stress at the wall can be corrected as

$$\tau_w^c = \frac{R\Delta p}{2(L + \varepsilon R)} \quad (11.43)$$

where ε is an empirical parameter obtained by extrapolating a plot of Δp versus the capillary aspect ratio, L/R , to zero pressure drop at constant $\dot{\gamma}$ for capillaries of different lengths as shown in Figure 11-26. Procedures for incorporating the effects of viscous heating and pressure on capillary flow have been proposed [13, 14] but are not usually undertaken.

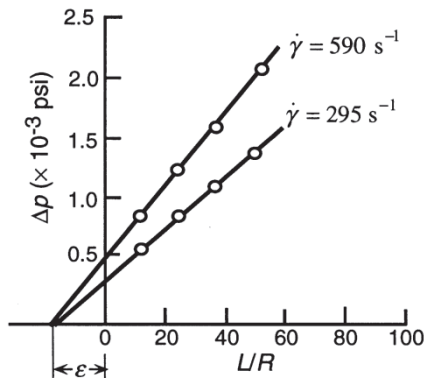


Figure 11-26 Bagley plot of pressure drop along a capillary versus capillary aspect ratio, L/R , at two different values of $\dot{\gamma}$. Adapted by special permission from M. H. Wohl, *Instruments for Viscosity*. Chemical Engineering, March 25, 1968. p. 99–104. Copyright © 1968, by Access Intelligence, New York 10005.

11.4.2 Couette Rheometer

Another example of a simple shear flow is circular Couette flow whereby a cylinder of radius R_i is driven at a constant angular velocity of Ω (usual units of rad s^{-1}) within an outer concentric cylinder of radius R_o as illustrated in Figure 11-27.

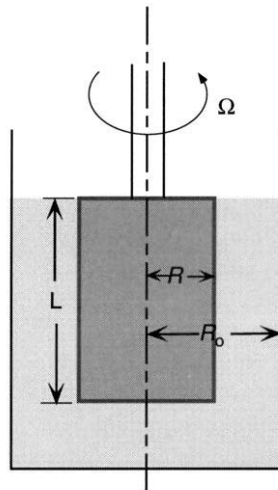


Figure 11-27 Couette rheometer.

The solution to this flow problem is simplified by using cylindrical coordinates and assuming that the cylinders have infinite length so that edge effects can be neglected.* Using the assumption of nonslip of the fluid at the surface of the two cylinders, the boundary conditions are

$$u_\theta(r = R_i) = R_i\Omega \quad (11.44)$$

and

$$u_\theta(r = R_o) = 0. \quad (11.45)$$

Unlike the case for plane Couette flow, the velocity profile is dependent upon the rheological properties of the fluid. The general solution for the θ component of the velocity vector for a PLF (eq. (11.13)) is

$$\frac{u_\theta}{R_i\Omega} = \left(\frac{r}{R_i} \right) \frac{1 - (R_o/r)^{2/n}}{1 - \kappa^{-2/n}} \quad (11.46)$$

where $\kappa = R_i/R_o$ is the aspect ratio. Again, this is an example of a viscometric flow where the remaining components of the velocity vector (i.e., u_r and u_z) are zero. For a Newtonian fluid ($n = 1$) such as water or mineral oil, eq. (11.46) reduces to

$$u_\theta = \frac{\Omega R_i^2}{R_i^2 - R_o^2} \left(r - \frac{R_o^2}{r} \right). \quad (11.47)$$

The expressions for shear stress and shear rate are

$$\tau = \frac{M}{2\pi r^2 L} \quad (11.48)$$

and

$$\dot{\gamma} = \frac{2\Omega R_i^2 R_o^2}{r^2 (R_i^2 - R_o^2)} \quad (11.49)$$

where M is the measured torque and L is the (submerged) length of the inner cylinder.

* Corrections can be made for edge effects by taking data for cylinders of different lengths in a manner similar to the Bagley correction for capillary data.

11.4.3 Cone-and-Plate Rheometer

Another important method of measuring the rheological properties of polymer solutions and melts is the cone-and-plate rheometer, which is illustrated in Figure 11-28. Either steady-shear or dynamic-viscosity data (see Section 5.1.3) can be obtained by this method. The cone angle, β , is typically very small (1 to 3 radians)—much smaller than is suggested by Figure 11-28. At these low angles, the shear rate is given as

$$\dot{\gamma} = \frac{\Omega}{\beta} \quad (11.50)$$

where Ω is the angular velocity of the cone. Dynamic viscosity can be obtained by applying an oscillatory shear on the cone. The shear stress, τ , is determined as

$$\tau = \frac{3M}{2\pi R_c^3} \quad (11.51)$$

where M is the measured torque on the cone having radius R_c . The apparent viscosity is then obtained from steady-shear measurements as

$$\eta = \frac{\tau}{\dot{\gamma}} \quad (11.52)$$

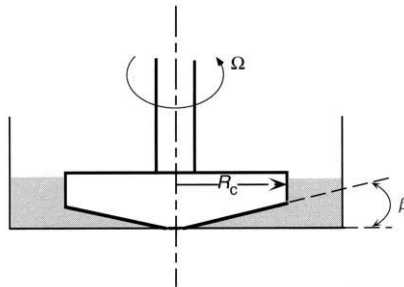


Figure 11-28 Idealized illustration of a cone-and-plate rheometer.

11.4.4 Rheometry of Polymer Solutions and Melts

Cone-and-plate, Couette cylinder, and also parallel-plate and eccentric rotating-plate rheometers can measure apparent viscosity over a low to moderate range of shear rates (e.g., 10^{-4} to 10^3 s $^{-1}$). Slit and capillary rheometers operate at high shear rates typical of many processing operations such as extrusion (see Table 11-2). Measurements using a variety of rheometers (e.g., cone-and-plate, slit, and capillary

rheometers) can be used to cover the entire range of shear rates, as illustrated in Figure 11-29.

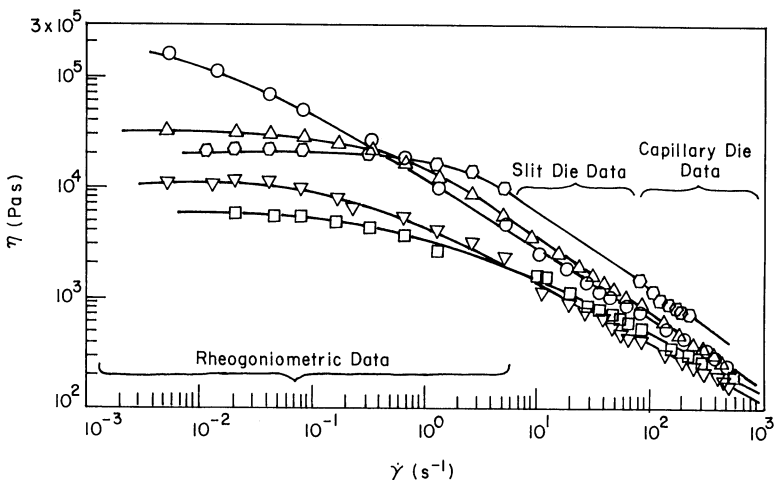


Figure 11-29 Viscosity versus shear rate for polymer melts at 200°C showing ranges of shear rate over which rheogoniometric (cone-and-plate), slit-die, and capillary rheometric measurements apply. Data for (○) high-density polyethylene, (Δ) polystyrene, (□) poly(methyl methacrylate), (▽) low-density polyethylene, and (□) polypropylene. Reprinted from C. D. Han, *Rheology in Polymer Processing*. 1976, New York: Academic Press. p. 108. Copyright 1976, Academic Press.

11.5 Modeling of Polymer-Processing Operations

11.5.1 Extrusion

Most complex polymer-processing operations can be reduced to a number of simple flow operations (see Section 11.3), which can be more easily solved. This is true for processing operations such as wire coating, blow molding, calendering, extrusion, and others. A full discussion of the modeling of polymer-processing operations is beyond the scope of this chapter and the reader is encouraged to consult any of a number of excellent texts cited in the Suggested Reading at the end of this chapter. As an illustration of the general approach, the basics of the modeling of extrusion are given in this section.

As discussed in Section 11.1.1, an extruder has three zones—feed, compression, and metering. In the modeling of extrusion, the metering section is the easiest

to analyze because the screw is conveying a homogeneous melt compared to solid pellets in the feed zone and a complex mixture of pellets and molten polymer in the compression zone. Clearly, a complete modeling of the extrusion process requires a coupled analysis of all three zones; however, the simpler treatment required to model the metering zone serves to illustrate how basic rheological principles developed in Sections 11.2 and 11.3 can be applied to tackle more complex processing problems.

To analyze flow in the metering zone, an approximation that is made (i.e., the lubrication approximation) is that rotation of the screw in the extruder shears the melt along the screw channel in a manner similar to plane Couette flow (Section 11.3.2) as described below. When no die is attached to the extruder, shear flow is the only consideration and the modeling is particularly easy. This is called a condition of *open discharge*. When a die (e.g., capillary, slit, or annular) is attached to the extruder, a pressure drop is produced across the die (pressure flow) and flow through the extruder is a combination of shear flow along the screw channel and pressure flow (back flow) against the extrusion direction. The volumetric flow, Q , therefore can be expressed as a simple combination of drag (shear) and pressure flows as^{*}

$$Q = Q_d - Q_p. \quad (11.53)$$

From eq. (11.53), it is clear that the case of open discharge (i.e., $Q_p = 0$) results in the maximum extruder output. Simple pressure flow through various die geometries has been discussed in Section 11.3.1. Expressions were given for isothermal flow of both Newtonian and power-law fluids. In these cases, Q was given as some function of the pressure drop across the die (see Table 11-3). These relationships were called the die characteristics.

In order to obtain an expression for a screw characteristic (Q versus Δp), it is necessary to make some assumptions about the extruder screw geometry that allow the flow to be modeled as plane Couette flow. An illustration of a simple screw geometry is shown in Figure 11-30. If the diameter of the screw, D , is much greater than the channel depth, B ,[†] and the screw is assumed to have constant depth along the extruder barrel, the screw channel can be visually unwrapped from the screw barrel to give a long rectangular channel, as illustrated in Figure 11-31. Drag flow along the screw channel can then be modeled as plane shear flow with the barrel wall shearing fluid in the channel. Due to the presence of the channel walls, the flow is not a simple flow such as plane Couette flow between two infinitely wide

^{*} Back flow due to leakage between the top of the screw flight and barrel wall is usually neglected. This expression is strictly true for Newtonian fluids for which the two flows are not coupled as they would be in the case of non-Newtonian flow.

[†] The flight clearance, δ , is usually considered to be negligible with respect to B .

parallel plates as discussed in Section 11.3.2. Plane Couette flow may be a reasonable assumption, however, if the width, W , of the channel is much greater than the channel height, B .

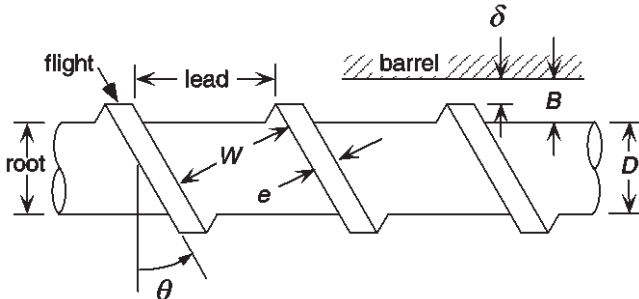


Figure 11-30 Illustration of extruder-screw geometry. Adapted from S. Middleman, *Fundamentals of Polymer Processing*. 1977, New York: McGraw-Hill Book Company. Reproduced with permission of Stanley Middleman.

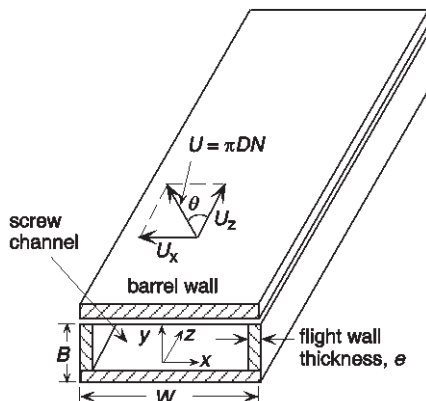


Figure 11-31 Geometry of an unwrapped screw channel.

In order to simplify the analysis of the extrusion process, the flow can be assumed to be isothermal and the fluid to be Newtonian. Under these conditions and using the geometric approximations that $W \gg B$ and $D \gg B$, the screw characteristic, a combination of both drag and pressure flows along the screw channel, is given as

$$Q = AN - C \frac{\Delta P}{\mu} \quad (11.54)$$

where N is the screw speed (in rpm) and μ is the Newtonian viscosity. The parameters A and C are determined by the geometry of the screw (see Figure 11-30) as

$$A = \frac{1}{2} \pi D W B \cos \theta \quad (11.55)$$

and

$$C = \frac{WB^3}{12Z} \quad (11.56)$$

where Z is the screw channel length, which is related to the overall length of the extruder, L , and angle of the flight, θ , as

$$Z = \frac{L}{\sin \theta}. \quad (11.57)$$

For Newtonian fluids, the die characteristic can be put in the general form

$$Q = \frac{k}{\mu} \Delta p \quad (11.58)$$

where k is a function of the geometry for a given die (e.g., capillary, annulus, or slit), as given in Table 11-4. For Newtonian fluids, the die characteristic is a linear function of Δp , as was the screw characteristic. A plot of Q versus Δp for the screw (eq. (11.54)) and that for the die (eq. (11.58)) will intersect at a point that defines the *operating parameters* of Q and Δp for the combined operation of the extruder and die. Alternatively, Δp can be obtained analytically for extrusion of a Newtonian fluid by employing the mass balance between the extruder and die

$$Q_{\text{extruder}} = Q_{\text{die}}. \quad (11.59)$$

Substitution of eqs. (11.54) and (11.58) into eq. (11.59) gives the operating pressure drop as

$$\Delta p = \frac{\mu AN}{k + C}. \quad (11.60)$$

Once Δp is obtained from eq. (11.60), Q can then be calculated from either eq. (11.54) or eq. (11.58).

The *power* consumption for extrusion of a Newtonian fluid under isothermal conditions is given as

$$P = E \mu N^2 Z + AN \Delta p \quad (11.61)$$

where Δp is the operating pressure and E is a parameter determined from the screw geometry as

$$E = \left(\frac{\pi^3 D^3}{B} \right) \sin \theta (1 + 3 \sin^2 \theta). \quad (11.62)$$

Table 11-4 Die Parameters, k

Die	Expressions for k
Capillary	$\pi R^4 / 8L$
Annulus	$(\pi R_o^4 / 8L) \left[1 - \kappa^4 - \frac{(1 - \kappa^2)^2}{\ln(1/\kappa)} \right]$
Slit ^a	$WH^3 F_p / 12L$

^a F_p is a shape factor that is an infinite series as a function of the aspect ratio, W/H ; F_p goes to unity in the limit as W/H goes to zero (equivalent to pressure flow through infinitely wide parallel plates).

Alternatively, the screw characteristic may be expressed in a dimensionless form by defining the variables

$$\Pi_Q = \frac{Q}{U_z BW} \quad (11.63)$$

and

$$\Pi_p = \frac{\Delta p B^2}{\mu U_z Z} \quad (11.64)$$

where U_z is the linear velocity of the screw barrel along the screw channel (the z -direction), given as

$$U_z = \pi D N \cos \theta. \quad (11.65)$$

In the case of a Newtonian fluid in isothermal flow, a plot of Π_Q versus Π_p is linear, as shown in Figure 11-31. The limiting case of open discharge, which provides the maximum extruder output, is given by $\Pi = 0$ for which $\Pi = 1/2$, as shown by the plot of Figure 11-32. This means that Q for open discharge in Newtonian flow is

$$Q = \frac{1}{2} U_z BW \quad (11.66)$$

which is the equivalent expression for drag Couette flow of a Newtonian fluid between two infinitely wide, parallel plates (eq. (11.31)). In the case of the extruder,

the two parallel plates are taken to be the bottom of the screw channel and the inner surface of the extruder barrel (where the lubrication approximation has been made that $W \gg B$ and $D \gg B$).

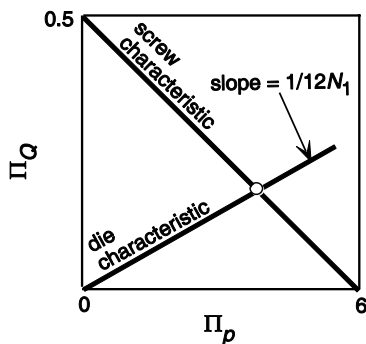


Figure 11-32 Plot of dimensionless screw and die characteristics for isothermal Newtonian flow. Adapted from S. Middleman, *Fundamentals of Polymer Processing*. 1977, New York: McGraw-Hill Book Company. Reproduced with permission of Stanley Middleman.

The die characteristic for isothermal Newtonian flow can also be put in dimensionless form as

$$\Pi_Q = \frac{\Pi_p}{12N_1} \quad (11.67)$$

where N_1 is given as

$$N_1 = \frac{C}{k} \quad (11.68)$$

In eq. (11.68), C is a function of screw geometry (eq. (11.56)) and k is a function of the die geometry, as given in Table 11-4. The dimensionless die characteristic is included in the plot of the screw characteristic shown in Figure 11-32. For given die and screw geometries, Newtonian viscosity, and screw speed, the intersection of the dimensionless screw and die characteristics defines the operating parameters of volumetric screw output, Q , and pressure drop, Δp . This information can then be used to determine the power requirement for the extruder given by eq. (11.61).

The assumptions of both isothermal and Newtonian flow may be viewed as rather extreme for the modeling of the extrusion of a non-Newtonian fluid; however, they form a reasonable basis for refinement. As was given in Table 11-3, die characteristics are available for the isothermal flow of power-law fluids. Numerical solutions are also available for combined pressure and drag flow of a PLF in a chan-

nel. From this information, the screw characteristics for PLF flow can be obtained as shown in dimensionless form in Figure 11-32.

As shown, the relationship between Π_o and Π_p is no longer linear except in the case when the power-law index, n , is unity; this is the limiting case for isothermal Newtonian flow, as illustrated in Figure 11-33. Similar nonlinearity would follow for the die characteristics and, therefore, an analytical solution for Δp as given in eq. (11.60) for a Newtonian fluid is not possible. In the graphical solution, the intersection of the dimensionless die and screw characteristics defines the operating parameters, Q and Δp , for the combination of extruder and die, as illustrated for Newtonian fluid flow in Figure 11-32. Further refinements to include adiabatic flow of a power-law fluid in the screw channel have also been made and give a better picture of actual extrusion operation.

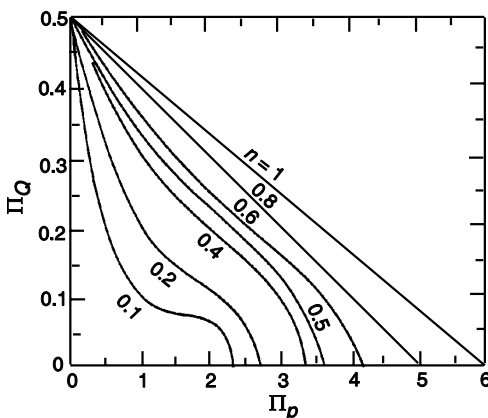


Figure 11-33 Dimensionless screw characteristics for isothermal power-law flow. Adapted from S. Middleman, *Fundamentals of Polymer Processing*. 1977, New York: McGraw-Hill Book Company. Reproduced with permission of Stanley Middleman.

11.5.2 Wire Coating

To coat a wire with an insulating polymer coating, a bare copper wire is pulled through a capillary die attached to an extruder. As a first approximation, wire coating can be modeled as axial annular drag flow as illustrated in Figure 11-34. A solution can be obtained for both Newtonian and non-Newtonian fluids with or without an imposed pressure drop. The objective of this analysis is to obtain an expression for the thickness of the coating, h , given the geometry (i.e., length, L , and diameter, D) of the die channel, the operating parameters of the die (e.g., temperature and axial velocity of the wire, U), and the properties of the fluid (e.g., viscosity at a specif-

ic temperature and shear rate in the case of a non-Newtonian fluid). Alternatively, analysis of this operation can provide insight into how changes in different operational or design parameters can affect the final coating thickness of the insulation or how parameters must be set to achieve a specified thickness. The most realistic but most difficult problem is annular drag flow of a PLF under a pressure drop; however, the simpler case of annular drag flow of a Newtonian fluid under conditions of open discharge as developed below serves to illustrate the general approach to this modeling problem.

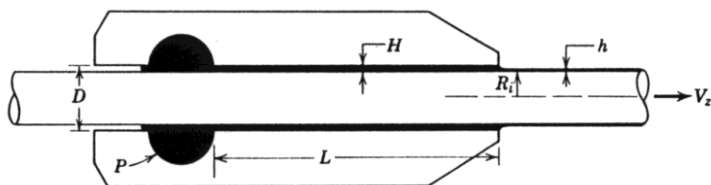


Figure 11-34 Representation of a wire-coating operation. Reproduced from J. M. McKelvey, *Polymer Processing*. 1962, New York: Wiley & Sons, with permission of James M. McKelvey.

The mass flow rate of the coating, \dot{m}_c , can be obtained as

$$\dot{m}_c = V_z A_c \rho \quad (11.69)$$

where V_z is the axial velocity of the wire through the die, ρ is the density of the coating at the temperature at the outlet of the die, and A_c is the cross-sectional area of the coating. Given the radius of the wire, R_i , and the thickness of the coating, h , eq. (11.69) becomes

$$\dot{m}_c = V_z S \left[(R_i + h)^2 - R_i^2 \right] \rho \quad (11.70)$$

A mass balance equates the mass flow rate of the extruded coating with the mass flow rate due to drag flow in the die

$$\dot{m}_d = \rho' Q \quad (11.71)$$

where ρ' is the polymer density at the temperature *inside* the die and Q is the volumetric flow rate due to axial annular drag flow of the wire in the die. The solution for Q of a PLF was given in eq. (11.36). As indicated in Section 11.3.2, it is not possible to get Q for a Newtonian fluid directly from eq. (11.36) simply by setting $n = 1$. The actual solution for a Newtonian fluid is given as

$$Q = -2\pi R(R - R_i) \frac{2\kappa^2 \ln \kappa - \kappa^2 + 1}{4(1-\kappa) \ln \kappa} \quad (11.72)$$

where

$$\kappa = \frac{R}{R_i} . \quad (11.73)$$

Substitution of eq. (11.73) into eq. (11.72) and then equating the mass flow rate ($\dot{m}_c = \dot{m}_d$) give a quadratic equation whose solution is

$$h' = \frac{h}{R_i} = \left[1 - \frac{2\rho'}{\kappa\rho} \left(\frac{1}{\kappa} - 1 \right) F(\kappa) \right]^{1/2} - 1 \quad (11.74)$$

where h' is a dimensionless coating thickness and

$$F(\kappa) = \frac{2\kappa^2 \ln \kappa - \kappa^2 + 1}{4(1-\kappa) \ln \kappa} . \quad (11.75)$$

An interesting result revealed by eq. (11.74) is that the coating thickness for a Newtonian fluid is primarily a function of die and wire diameters but is independent of wire velocity and the fluid viscosity.

For a PLF, the dimensionless thickness for isothermal flow is given by

$$h' = \left[1 - \frac{2\rho'}{\kappa\rho} \left(\frac{1}{\kappa} - 1 \right) H(\kappa, q) \right]^{1/2} - 1 \quad (11.76)$$

where

$$H(\kappa, q) = \frac{1}{q+2} \frac{1 - \kappa^{q+2}}{(1-\kappa)(\kappa^q - 1)} - \frac{1 + \kappa}{2(\kappa^q - 1)} \quad (11.77)$$

and

$$q = 1 - \frac{1}{n} . \quad (11.78)$$

Again, coating thickness is independent of wire velocity but now depends upon the power-law index, n , (i.e., viscosity) of the fluid. As temperature increases, it would be expected that n should increase (i.e., become less shear thinning) and, therefore, h' should increase.

In the case of both combined drag and pressure flow, the total volumetric flow is additive ($Q = Q_d + Q_p$) for a Newtonian fluid only. The solution to this problem shows that increasing pressure drop across the die increases the coating thickness. The result for a PLF is a bit more difficult to obtain as it requires a solution to the dynamic equations (see Appendix A.2) for u_z . Solutions are available in many poly-

mer processing texts such as the excellent one cited in the Suggested Reading at the end of this chapter.

APPENDICES

A.1 RELATIONSHIP BETWEEN THE WLF PARAMETERS AND FREE VOLUME

The Doolittle equation [15, 16] relates viscosity to the fractional free volume, f , which is defined as

$$f = \frac{V_f}{V} \quad (\text{A.1})$$

where V is the actual volume of the polymer at some temperature, T . The Doolittle equation is given as

$$\ln \eta(T) = \ln A + B \left(\frac{1}{f} - 1 \right) \quad (\text{A.2})$$

where A and B are constants. The corresponding equation for $T = T_g$ is then

$$\ln \eta(T_g) = \ln A + B \left(\frac{1}{f_g} - 1 \right) \quad (\text{A.3})$$

where f_g is the fractional free volume at T_g . The fractional free volume, f , at a given temperature, T , is related to f_g as

$$f = f_g + \alpha_f (T - T_g) \quad (\text{A.4})$$

where α_f is the thermal-expansion coefficient of the free volume

$$\alpha_f = \left(\frac{\partial V_f}{\partial T} \right)_p . \quad (\text{A.5})$$

Substitution of eqs. (A.2) to (A.4) into eq. (11.7) gives

$$\log a_T = \log \frac{\eta(T)}{\eta(T_g)} = - \left(\frac{B}{2.303 f_g} \right) \left[\frac{T - T_g}{(f_g / \alpha_f) + T - T_g} \right]. \quad (\text{A.6})$$

Comparison of the form of eq. (A.6) with the WLF expression (eq. 5.127) for $\log a_T$ gives the following relationships for the WLF parameters:

$$C_1 = \frac{B}{2.303 f_g} \quad (\text{A.7})$$

and

$$C_2 = \frac{f_g}{\alpha_f} . \quad (\text{A.8})$$

Since the thermal-expansion coefficient of free volume is not generally available,^{*} the thermal-expansion coefficient of the melt, easily determined by dilatometry (Section 4.3.2), may be used.

A.2 DYNAMIC AND CONTINUITY EQUATIONS

A.2.1 CARTESIAN COORDINATES

x-Component:

$$\rho \left(\frac{\partial u_x}{\partial t} + u_x \frac{\partial u_x}{\partial x} + u_y \frac{\partial u_x}{\partial y} + u_z \frac{\partial u_x}{\partial z} \right) = -\frac{\partial p}{\partial x} + \left(\frac{\partial \tau_{xx}}{\partial x} + \frac{\partial \tau_{yx}}{\partial y} + \frac{\partial \tau_{zx}}{\partial z} \right) + \rho g_x \quad (\text{A.9})$$

y-Component:

$$\rho \left(\frac{\partial u_y}{\partial t} + u_x \frac{\partial u_y}{\partial x} + u_y \frac{\partial u_y}{\partial y} + u_z \frac{\partial u_y}{\partial z} \right) = -\frac{\partial p}{\partial y} + \left(\frac{\partial \tau_{xy}}{\partial x} + \frac{\partial \tau_{yy}}{\partial y} + \frac{\partial \tau_{zy}}{\partial z} \right) + \rho g_y \quad (\text{A.10})$$

z-Component:

$$\rho \left(\frac{\partial u_z}{\partial t} + u_x \frac{\partial u_z}{\partial x} + u_y \frac{\partial u_z}{\partial y} + u_z \frac{\partial u_z}{\partial z} \right) = -\frac{\partial p}{\partial z} + \left(\frac{\partial \tau_{xz}}{\partial x} + \frac{\partial \tau_{yz}}{\partial y} + \frac{\partial \tau_{zz}}{\partial z} \right) + \rho g_z \quad (\text{A.11})$$

Continuity equation:

$$\frac{\partial u_x}{\partial x} + \frac{\partial u_y}{\partial y} + \frac{\partial u_z}{\partial z} = 0 \quad (\text{A.12})$$

A.2.2 CYLINDRICAL COORDINATES

r-Component:

* Although the thermal expansion coefficient of free volume can be obtained by positron annihilation spectroscopy and from molecular simulation, data are extremely limited at this time.

$$\rho \left(\frac{\partial u_r}{\partial t} + u_r \frac{\partial u_r}{\partial r} + \frac{u_\theta}{r} \frac{\partial u_r}{\partial \theta} - u_z \frac{\partial u_r}{\partial z} \right) = - \frac{\partial p}{\partial r} \quad (\text{A.13})$$

***θ*-Component:**

$$\begin{aligned} \rho \left(\frac{\partial u_\theta}{\partial t} + u_r \frac{\partial u_\theta}{\partial r} + \frac{u_\theta}{r} \frac{\partial u_\theta}{\partial \theta} - \frac{u_r u_\theta}{r} + u_z \frac{\partial u_\theta}{\partial z} \right) &= - \frac{1}{r} \frac{\partial p}{\partial \theta} \\ &+ \left[\frac{1}{r^2} \frac{\partial}{\partial r} (r^2 \tau_{r\theta}) + \frac{1}{r} \frac{\partial \tau_{\theta\theta}}{\partial \theta} + \frac{\partial \tau_{\theta z}}{\partial z} \right] + \rho g_\theta \end{aligned} \quad (\text{A.14})$$

***z*-Component:**

$$\rho \left(\frac{\partial u_z}{\partial t} + u_r \frac{\partial u_z}{\partial r} + \frac{u_\theta}{r} \frac{\partial u_z}{\partial \theta} + u_z \frac{\partial u_z}{\partial z} \right) = - \frac{\partial p}{\partial z} + \left[\frac{1}{r} \frac{\partial}{\partial r} (r \tau_{rz}) + \frac{1}{r} \frac{\partial \tau_{\theta z}}{\partial \theta} + \frac{\partial \tau_{zz}}{\partial z} \right] + \rho g_z \quad (\text{A.15})$$

Continuity equation:

$$\frac{1}{r} \frac{\partial}{\partial r} (r u_r) + \frac{1}{r} \frac{\partial u_\theta}{\partial \theta} + \frac{\partial u_z}{\partial z} = 0 \quad (\text{A.16})$$

SUGGESTED READING

- Aharoni, S. M., *Critical Concentration for Intermolecular Interpenetration and Entanglements*. Journal of Macromolecular Science: Part B: Physics: 1978. **B15**: p. 347.
- Alberino, L. M., *Reaction Injection Molding: Review and Overview*. Polymer News, 1985. **11**: p. 135.
- Barnes, H. A., J. F. Hutton, and K. Walters, *An Introduction to Rheology*. 1989, Amsterdam: Elsevier.
- Choi, H. J., and M. S. Jhon, *Polymer-Induced Turbulent Drag Reduction*. Industrial and Engineering Chemistry Research, 1996. **35**: p. 2993.
- Darby, R. *Taking the Mystery Out of Non-Newtonian Fluids*. Chemical Engineering, March 2001, p. 66.
- Denn, M. M., *Extrusion Instabilities and Wall Slip*. Annual Review of Fluid Mechanics, 2001. **33**: p. 265.
- Han, C. D., *Rheology in Polymer Processing*. 1976, New York: Academic Press.
- McCrumb, N. G., C. P. Buckley, and C.B. Bucknall, *Principles of Polymer Engineering*. 1988, New York: Oxford University Press.
- McKelvey, J. M., *Polymer Processing*. 1962, New York: John Wiley & Sons.
- Middleman, S., *The Flow of High Polymers*. 1968, New York: Interscience Publishers.

- Middleman, S., *Fundamentals of Polymer Processing*. 1977, New York: McGraw-Hill Book Company.
- Morton-Jones, D. H., *Polymer Processing*. 1989, London: Chapman and Hall.
- Nielsen, L. E., *Polymer Rheology*. 1977, New York: Marcel Dekker, Inc.
- Tadmor, Z., and C. G. Gogos, *Principles of Polymer Processing*. 1979, New York: John Wiley & Sons.
- Walters, K., *Rheometry*. 1975, London: Chapman and Hall.
- Wilkes, G. L., *An Overview of the Basic Rheological Behavior of Polymer Fluids*. Journal of Chemical Engineering, 1981. **58**: p. 880.

PROBLEMS

11.1 Poly(vinyl acetate) (PVAc) is extruded at 180°C at constant temperature through a capillary rheometer having a ram (reservoir) diameter of 0.375 in. and a capillary with an inside diameter of 0.041 in. and length of 0.622 in. The data provided give the efflux time to extrude 0.0737 in.³ at different ram loads. Using the following data:

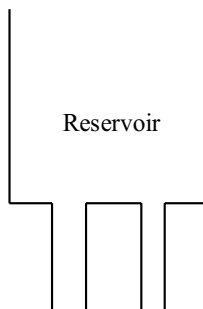
Ram Load (lb _f)	Efflux Time (min)
97.5	5.32
145	1.58
217	0.31
250	0.17

(a) Determine the power-law parameters n and m for PVAc and state all assumptions used to obtain your results.

(b) Plot the apparent viscosity, η , in units of Pa-s versus the nominal shear rate at the wall, $\dot{\gamma}_w$ (s⁻¹), using logarithmic coordinates.

11.2 Plot the dimensionless velocity profile for polystyrene flowing in a capillary at 483 K.

11.3 As illustrated, two capillaries of identical length are connected to the same liquid reservoir in which a power-law fluid is held. The tubes differ in radii by a factor of 2. When a pressure is applied to the reservoir, the volumetric flow rates from the two tubes differ by a factor of 40. What is the value of n ? How different are the nominal shear rates in the two cases?



11.4 Molten polystyrene flows through a circular tube at 210°C under a pressure drop of 1000 psi. Given that the inside diameter of the tube is 0.25 in. and that the tube is 3 in. in length, calculate the following:

- (a) The (nominal) shear stress at the wall in units of N m^{-2}
- (b) The (nominal) shear rate at the wall in s^{-1}
- (c) The volumetric flow rate in $\text{cm}^3 \text{ s}^{-1}$

Assume that flow is isothermal, steady, and fully developed.

11.5 (a) Given that tensile (Trouton's) viscosity is defined as

$$\eta_T = \frac{\sigma}{\dot{\varepsilon}}$$

where σ and $\dot{\varepsilon}$ are the *true* tensile stress and *true* strain, respectively, show that

$$\ln L = \left(\frac{1}{\eta_T} \right) \sigma t + \ln L_0$$

when viscosity is independent of $\dot{\varepsilon}$ and L_0 is the *initial* length of the sample.

(b) A strip of polyisobutylene (800,000 molecular weight) is subjected to a fixed tensile load at ambient conditions. Initially, the sample is 0.699 cm wide, 6.0 cm long, and 0.155 cm thick. The strip is hung vertically and a mass of 75 g is attached to the bottom of the strip. The sample length is then recorded as a function of time with the following measurements:

Time (min)	1	2	3	6	12	15	18	21	24
Length (cm)	6.90	7.00	7.10	7.25	7.48	7.60	7.69	7.79	7.90

Plot the data given in the form of $\ln L$ versus σt and determine the value of η_T in SI units. Comment on the probable phenomenological significance of the actual intercept of the plot obtained by extrapolating the linear portion of the data.

11.6 Show that eq. (11.37), which defines shear stress in pressure flow through a capillary, is correct by balancing pressure force and shear force in a cylindrical element.

11.7 A 2-in. melt extruder is pumping a *Newtonian fluid* through a slit die for which the form factor, F_p , is 0.5. The viscosity, μ , of the fluid at operating conditions is $0.2 \text{ lb}_f \text{s in.}^{-2}$. The dimensions of the slit die are 1 in. in width, 0.8 in. in height, and 3 in. in length. The geometric parameters for the extruder are given in the following table:

Extruder Geometry	
Extruder length, L_{ext}	14.75 in.
Screw diameter, D	1.982 in.
Channel depth, B	0.166 in.
Flight angle, θ	30°
Channel width, W	11 in.

If the extruder is rotating at 60 rpm under isothermal conditions, determine the following:

(a) Pressure drop, Δp , in psi

(b) Volumetric flow rate, Q , in units of $\text{in.}^3 \text{ min}^{-1}$

(c) Power, P , required to operate the extruder in hp ($1 \text{ hp} = 550 \text{ ft-lb}_f \text{ s}^{-1}$)

11.8 Using the dynamic equations for cylindrical coordinates given in Appendix A.2.2 of this chapter, show how eq. (11.23) can be obtained making the usual assumptions of isothermal, steady, fully developed, laminar flow through a capillary. State any additional assumptions necessary to obtain eq. (11.23).

11.9 Derive eq. (11.25) for the velocity profile of a power-law fluid for pressure flow through a capillary.

11.10 Derive eq. (11.46) for the velocity u_θ of a power-law fluid in a Couette rheometer.

11.11 Derive eqs. (11.72) and (11.74) for the axial annular Couette flow of a Newtonian fluid in a wire-coating die.

11.12 A Newtonian fluid having a viscosity of 15,000 poise is to be coated on a wire having a diameter of 0.06 in. through an annular die of 0.08-in. inside diameter. The length of the die is 1.25 in. Assuming isothermal flow, calculate the required pressure drop (in psi) across the die to produce a uniform coating having a thickness of 0.06 in. The wire is moving at a velocity of 100 ft min^{-1} . What is the nominal shear rate in the die?

11.13 Derive eq. (11.76) for a PLF in a wire-coating operation.

REFERENCES

1. Baekeland, L. H., *The Synthesis, Constitution, and Uses of Bakelite*. Journal of Industrial and Engineering Chemistry, 1909. **1**: p. 149–161.
2. Lomellini, P., *Viscosity-Temperature Relationships of a Polycarbonate Melt: Williams-Landel-Ferry versus Arrhenius Behaviour*. Makromolekulare Chemie, 1992. **193**: p. 69–79.
3. Cohen, M. H. and D. Turnbull, *Molecular Transport in Liquids and Glasses*. Journal of Chemical Physics, 1959. **31**(5): p. 1164–1169.
4. Mewis, J., *Thixotropy—A General Review*. Journal of Non-Newtonian Fluid Mechanics, 1979. **6**: p. 1–20.
5. Wang, C. S. and J. R. Fried, *Viscoelastic Properties of Concentrated Cellulose Acetate Solutions*. Journal of Rheology, 1992. **36**(5): p. 929–945.
6. Onogi, S., et al., *Effects of Molecular Weight and Concentration on Flow Properties of Concentrated Polymer Solutions*. Journal of Polymer Science, Polymer Symposium, 1966. **15**(1): p. 381–406.
7. Carreau, P. J., *Rheological Equations from Molecular Network Theories*. PhD Dissertation, Department of Chemical Engineering, University of Wisconsin. 1992.
8. Wang, S.-Q., P. A. Drda, and Y.-W. Inn, *Exploring Molecular Origins of Sharkskin, Partial Slip, and Slope Change in Flow Curves of Linear Low Density Polyethylene*. Journal of Rheology, 1996. **40**(5): p. 875–898.
9. Pudjianto, S. and M. M. Denn, *A Stable “Island” in the Slip-Stick Region of Linear Low-Density Polyethylene*. Journal of Rheology, 1994. **38**(6): p. 1735–1744.
10. Toms, B. A., *Observations on the Flow of Linear Polymer Solutions through Straight Tubes at Large Reynolds Numbers*. Proceedings of the International Congress on Rheology, 1948. **2**: p. 135–141.
11. Burger, E. D., L. G. Chorn, and T. K. Perkins, *Studies of Drag Reduction Conducted over a Broad Range of Pipeline Conditions When Flowing Prudhoe Bay Crude Oil*. Journal of Rheology, 1980. **24**: p. 603–636.
12. Bagley, E. B., *End Corrections in the Capillary Flow of Polyethylene*. Journal of Applied Physics, 1957. **28**(5): p. 624–627.
13. Kamal, M. R. and H. Nyun, *Capillary Viscometry: A Complete Analysis Including Pressure and Viscous Heating Effects*. Polymer Engineering and Science, 1980. **20**(2): p. 109–119.
14. DeKee, D. and R. F. Wissbrun, *Polymer Rheology*. Physics Today, June 1998. p. 24–29.
15. Doolittle, A. K., *Studies in Newtonian Flow. II. The Dependence of the Viscosity of Liquids on Free Space*. Journal of Applied Physics, 1951. **22**(12): p. 1471–1475.
16. Doolittle, A. K., *Studies in Newtonian Flow. III. The Dependence of the Viscosity of Liquids on Molecular Weight and Free Space (in Homogeneous Series)*. Journal of Applied Physics, 1952. **23**(2): p. 236–239.

This page intentionally left blank